AD-A131 002 ETCHED CAVITY SAW (SURFACE ACOUSTIC WAVE) RESONATOR ELEMENTS FOR MULTIPOLE FILTER APPLICATIONS(U) R F MONOLITHICS INC DALLAS TX R J KANSY JUN 83 1/1

UNCLASSIFIED N00014-81-C-2304 F/G 20/1 NL

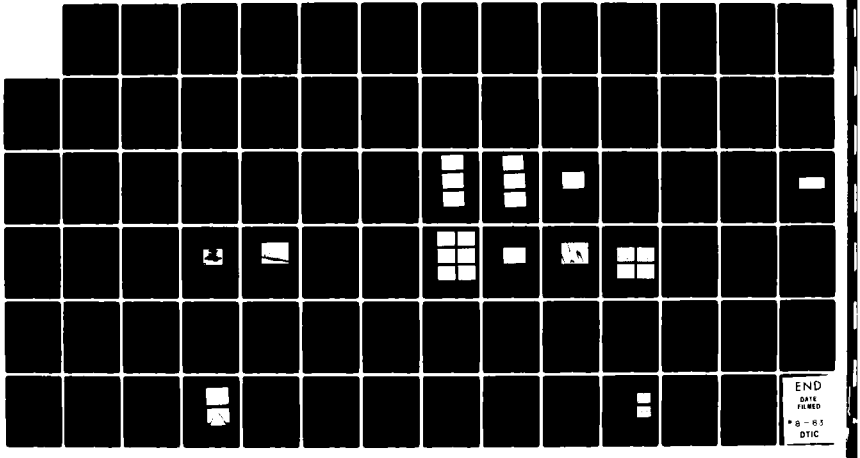

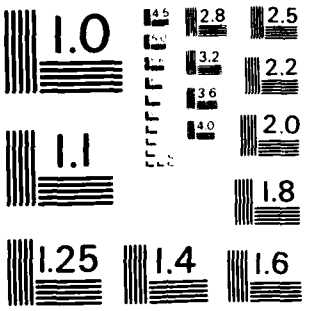

ETCHED CAVITY SAW RESONATOR ELEMENTS FOR MULTIPOLE FILTER APPLICATIONS

RF Monolithics, Inc.
4441 Sigma Road
Dallas, Texas 75234

June 1983

Final Technical Report for period
1 July 1981 - 28 February 1983

Prepared for

Naval Research Laboratory
4555 Overlook Avenue, S.W.
Washington, D. C. 20375

SECURITY CLASSIFICATION OF THIS PAGE (When Data Entered)

REPORT DOCUMENTATION PAGE		READ INSTRUCTIONS BEFORE COMPLETING FORM
1. REPORT NUMBER	2. GOVT ACCESSION NO. AD-A131 082	3. RECIPIENT'S CATALOG NUMBER
4. TITLE (and Subtitle) Etched Cavity SAW Resonator Elements for Multipole Filter Applications		5. TYPE OF REPORT & PERIOD COVERED Final Technical 6. PERFORMING ORG. REPORT NUMBER
7. AUTHOR(s) R.J. Kansy		8. CONTRACT OR GRANT NUMBER(s) N00014-81-C-2304
9. PERFORMING ORGANIZATION NAME AND ADDRESS RF Monolithics, Inc. 4441 Sigma Road Dallas, Texas 75234		10. PROGRAM ELEMENT, PROJECT, TASK AREA & WORK UNIT NUMBERS
11. CONTROLLING OFFICE NAME AND ADDRESS Naval Research Laboratory Washington, D.C. 20375		12. REPORT DATE June 1983 13. NUMBER OF PAGES 75
14. MONITORING AGENCY NAME & ADDRESS(if different from Controlling Office) Naval Research Laboratory Code 6853 Washington, D.C. 30275		15. SECURITY CLASS. (of this report) Unclassified 15a. DECLASSIFICATION DOWNGRADING SCHEDULE
16. DISTRIBUTION STATEMENT (of this Report) Approved for Public Release; Distribution unlimited		
17. DISTRIBUTION STATEMENT (of the abstract entered in Block 20, if different from Report)		
18. SUPPLEMENTARY NOTES		
19. KEY WORDS (Continue on reverse side if necessary and identify by block number) Surface Acoustic Wave Devices, Surface Acoustic Wave Resonators, Multipole Bandpass Filters		

20. ABSTRACT (Continue on reverse side if necessary and identify by block number)

The objective of this program is the evaluation of a unique Surface Acoustic Wave (SAW) resonator element proposed by RF Monolithics for application in multipole bandpass filters. The economical realization of multipole SAW resonator filters having steep skirts, low loss, and high out-of-band rejection requires the availability of SAW resonator elements having specific attributes: 1) reproducibility, 2) high coupling, 3) single moded, and 4) high Q. The resonator element studied during this program was invented

DD FORM 1 JAN 73 1473 EDITION OF 1 NOV 65 IS OBSOLETE

S/N 0102-LF-014-6601

SECURITY CLASSIFICATION OF THIS PAGE (When Data Entered)

to satisfy these requirements.

The key features of this new device are: 1) a uniform SAW velocity throughout the structure that reduces sensitivity to variations in the fabrication process, 2) independent realization of transduction and reflection functions that allow high coupling and good longitudinal mode suppression, and 3) a self-aligned multilevel process that eliminates critical alignments and promises high producibility in a volume manufacturing environment. The development of this device is an extension of the metal cavity resonator concept pioneered at RF Monolithics, and currently in volume production. The fabrication process incorporates a quartz etch step that is not required in the manufacture of the metal cavity units.

The most successful approach investigated during this program involved the use of an ion mill for the quartz etch. Since the ion mill also attacks aluminum, it was necessary to modify the process slightly, but the result remains a self-aligned process. Device performance in a 50 ohm system is limited by high insertion loss and low Q. The former is primarily due to the relatively high transducer impedance levels caused by an oversight in the initial device design, while the latter is tentatively attributed to redeposited material within the grooves. In all other respects it is in reasonable agreement with theory.

Table of Contents

List of Figures

List of Tables

I. INTRODUCTION

The objective of the program executed under Contract No. N00014-81-C- 2304 is the evaluation of a unique Surface Acoustic Wave (SAW) resonator element proposed by RF Monolithics for application in multipole bandpass filters. The economical realization of multipole SAW resonator filters having steep skirts, low loss, and high out-of-band rejection requires the availability of SAW resonator elements having specific attributes: 1) reproducibility, 2) high coupling, 3) single moded, and 4) high Q. The resonator element studied during this program was invented to satisfy these requirements.

The key features of this new device are: 1) a uniform SAW velocity throughout the structure that reduces sensitivity to variations in the fabrication process, 2) independent realization of transduction and reflection functions that allow high coupling and good longitudinal mode suppression, and 3) a self-aligned multilevel process that eliminates critical alignments and promises high producibility in a volume manufacturing environment. The development of this device is an extension of the metal cavity resonator concept pioneered at RF Monolithics, and currently in volume production. The fabrication process incorporates a quartz etch step that is not required in the manufacture of the

metal cavity units. However, the application of plasma quartz etch techniques in other laboratories implied that a major process development would not be required to achieve the etch uniformity required. Unfortunately, this implication was false, and a considerable part of the program was expended in an attempt to develop the requisite quartz etch process.

The most successful approach investigated during this program involved the use of an ion mill for the quartz etch. Since the ion mill also attacks aluminum, it was necessary to modify the process slightly, but the result remains a self-aligned process. Device performance in a 50 ohm system is limited by high insertion loss and low Q. The former is primarily due to the relatively high transducer impedance levels caused by an oversight in the initial device design, while the latter is tentatively attributed to redeposited material within the grooves. In all other respects it is in reasonable agreement with theory.

Section II of this report reviews the common multipole resonator filter elements and describes the etched cavity resonator concept in detail. Subsequent sections describe test device design and experimental results.

II. RESONATOR ELEMENTS FOR MULTIPOLE FILTERS

The most common SAW multipole resonator filter elements are one and two pole devices based on one of three basic two-port resonator structures shown in Fig. 1. Figure 1a shows the grooved reflector, recessed transducer configuration employed by Tanski [1-6]. The recessed transducer metallization is nearly reflectionless because of the close acoustic impedance match between quartz and aluminum. This allows the transducers to be optimally placed within the cavity to obtain maximum coupling to the cavity standing wave. However, the SAW velocities in the transducer and grating regions are intrinsically different, and variations in metal thickness can cause shifts in the resonant frequency relative to the grating stop band.

Figure 1b shows the grooved reflector, unrecessed transducer configuration employed by Cross, et al. [7] and Wise, et al. [8]. The transducer metallization causes substantial reflection, and the position of the transducers within the cavity must be adjusted to provide coherent reflections, not necessarily maximum coupling. This structure also exhibits dual SAW velocities, and is susceptible to variations in metal thickness or groove depth.

Figure 1c shows the metal cavity resonator structure produced

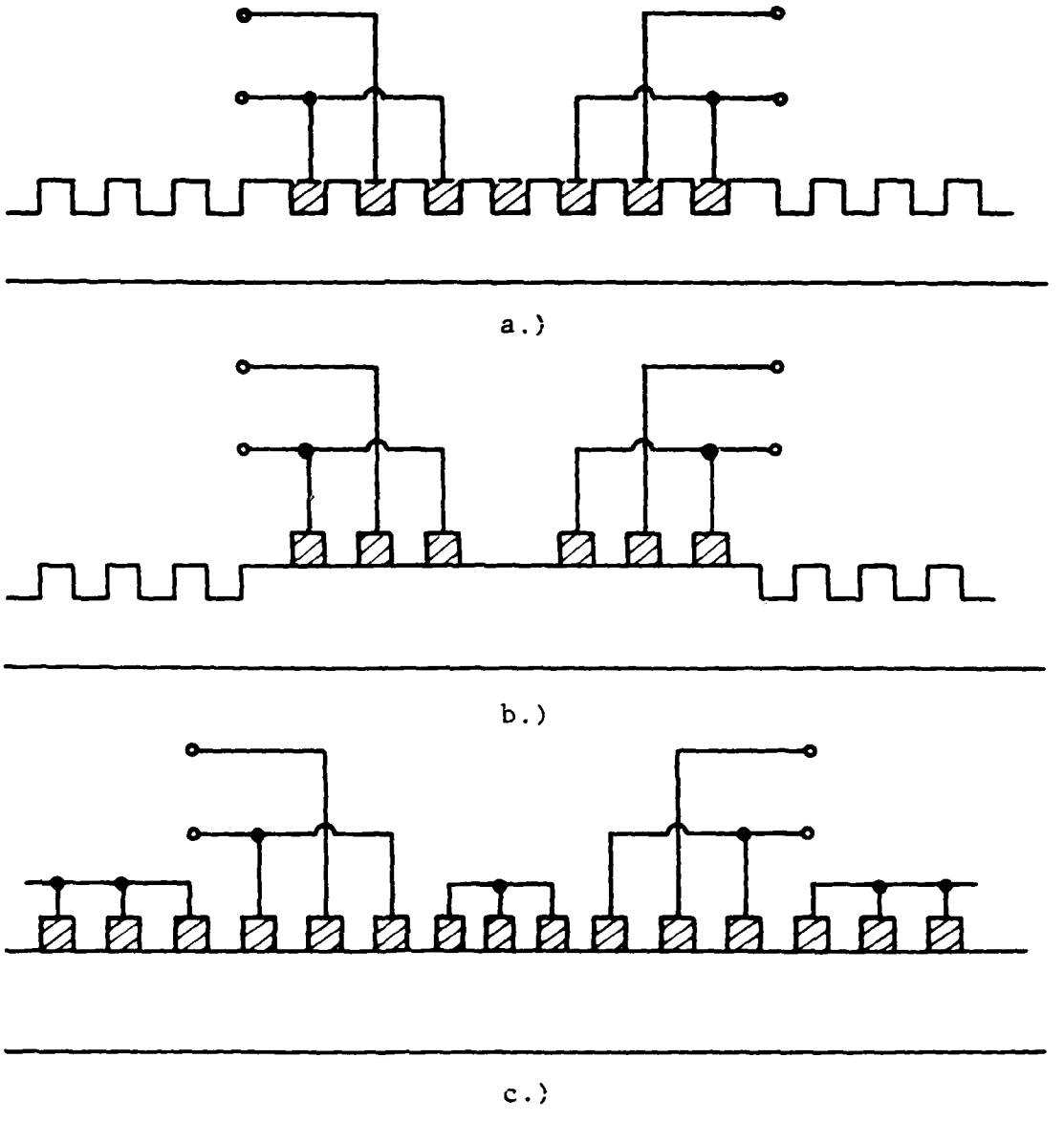

Figure 1. The three basic 2-port resonator structures.
a.) grooved reflector, recessed transducer,
b.) grooved reflector, unrecessed transducer,
c.) metal cavity.

at RF Monolithics. The reflective gratings are realized as shorted metal stripes, as opposed to the etched grooves employed above, and the transducers are effectively integrated within the gratings. In order that the primary resonance occur at the grating stop-band center frequency, the spacing between the gratings must be an integer number of half wavelengths. If the stripes in the center phasing section have the same dimensions as those in the gratings, then either abutting or eighth wavelength geometries are required. Instead, the periodicity changes very slightly in the phasing section to obtain the requisite grating spacing without incurring a drastic change in feature dimensions that would increase photolithographic resolution requirements. In addition this approach avoids the drastic change in reflection coefficient that has been associated with bulk mode scattering [9]. Most importantly, it results in a resonator structure having a uniform SAW velocity throughout the structure, reducing sensitivity to variations in fabrication parameters.

As-processed device yield information is typically sensitive, and very little has been published to date. Most of the literature pertaining to etched groove devices refer to individual trimming of devices by various processes to achieve a desired frequency tolerance. Bulst and Willibald [10] have published slice maps for their metal cavity r nators at 300 and 461 MHz that demonstrate standard

deviations of approximately 50 ppm. The authors attribute this variance to variations in the properties of the commercially available quartz substrates, specifically caused by varying growth conditions from the X and Z faces of the seed, which they display by means of an X-ray topograph of the mapped slice. They claim that 15 ppm variances have been obtained on defect free natural quartz substrates, presumably at the same center frequency.

Slice level testing at RF Monolithics shows that the standard deviation in center frequency for production metal cavity resonators in the frequency range of 500 to 700 MHz varies from approximately 50 ppm to 150 ppm, depending on metallization thickness. The standard deviation between adjacent devices is usually within confidence limits of the slice standard deviation, implying that the mechanism responsible for the variance has a characteristic dimension that is substantially smaller than the die size. Although variations in substrate properties may be of significance, the dependence on metallization thickness suggests that the effect of variations in stripe profile (through the stored energy effect) dominates current performance. It is anticipated that the achievement of device frequency accuracy of better than 25 to 50 ppm in a production environment without individual trimming requires the development of a fabrication process in which both film thickness and stripe profile are controlled to within a few percent of nominal

specifications.

The primary motivation for the use of etched grooves is the hope of obtaining better aging characterisitics than might be expected with deposited films. This hope is, as yet, unsubstantiated, and excellent aging results have been reported for metal cavity resonators [10]. It has been demonstrated that substantial aging effects are induced by metal migration effects at high dissipated power levels. Since the highest power level exists in the region between the reflective gratings, this effect will manifest itself primarily in the transducer metallization, which must be present in any of the structures.

Figure 2 compares the response of one pole, two port resonators for each of these structures. The symmetric response of the recessed transducer resonator is due to the independent realization of the transduction and reflection functions. Transducer stripes are placed at the peaks of the cavity standing wave providing maximum coupling to the primary mode. As shown in Appendix I, all SAW resonator structures are capable of supporting at least three longitudinal modes. The symmetry of the transducer placement in this case determines the coupling to the adjacent cavity modes having opposite symmetry. In two pole resonator elements it is straightforward to position each transducer symmetrically in each cavity to obtain suppression of the

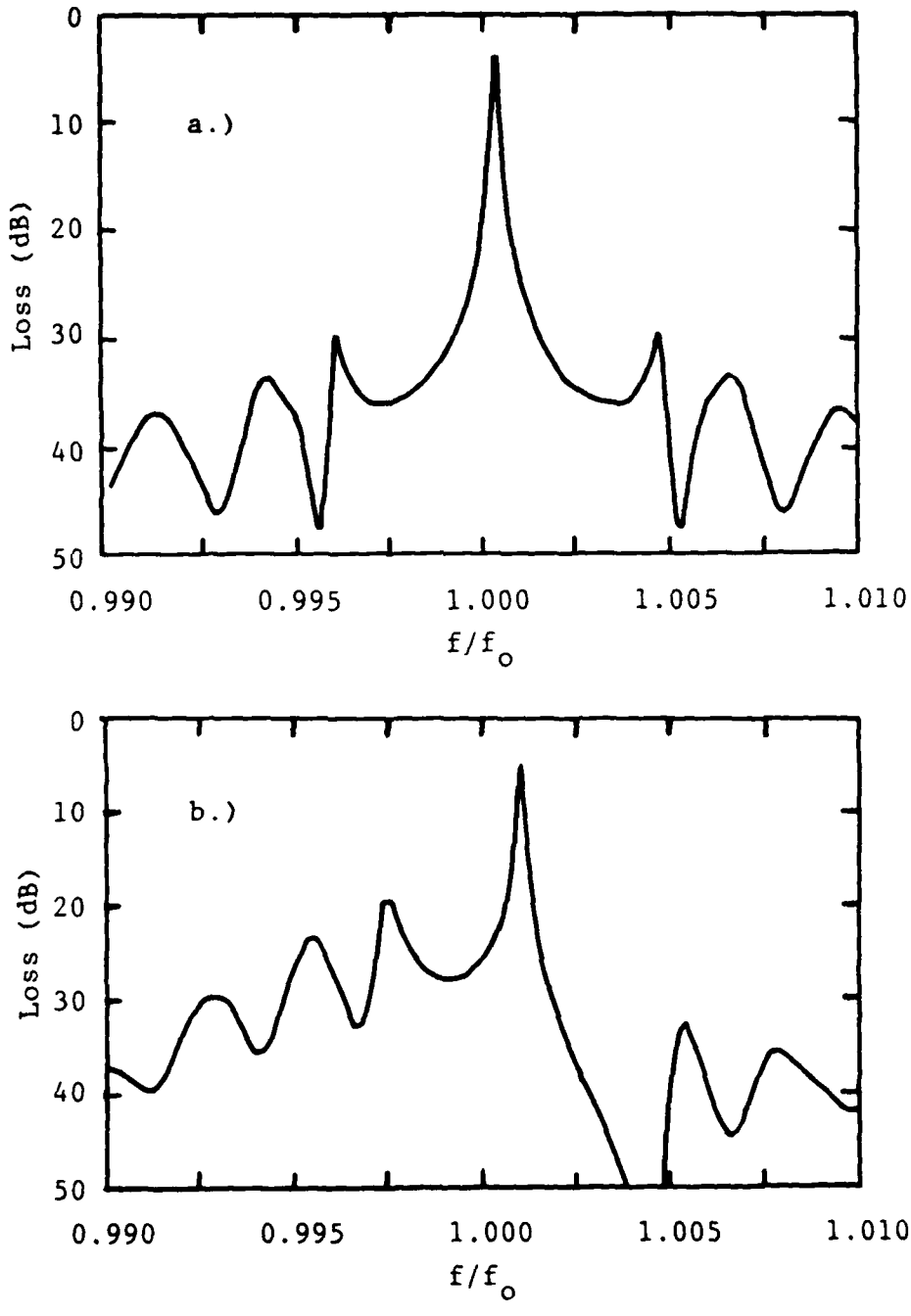

Figure 2. Typical 2-port frequency response. a.) Grooved cavity, b.) metal cavity.

adjacent modes. In one pole units, however, it requires splitting one of the transducers into two sections that must be interconnected around the other transducer. As shown in Appendix I it is always possible to prevent strong coupling to the higher order modes by reducing the groove depth. Of course, the grating length must be increased proportionately if the Q is to be maintained.

The unrecessed and metal cavity structures in Fig. 2 have similar non-symmetric responses due to the fixed relation between transducer and reflector stripes. Since the transducer stripes are no longer positioned at the peaks of the cavity standing wave, the adjacent cavity modes (opposite symmetry) near the reflector stop band edges can be strongly coupled. Since the effective grating spacing can be small, this is seldom the case. As shown in Appendix I, distortion of the transducer response due to internal reflections results in the observed spuria that represent a serious performance limitation to multipole resonator filters using the unrecessed or metal cavity elements. The relative level of the low frequency spurious in the metal cavity resonator is proportional to the ratio of transducer length to grating length for a fixed reflection coefficient. Thus, increasing transducer length to increase coupling in multipole applications causes a degredation in out-of-band rejection unless metal thickness is reduced and grating length increased proportionately.

The etched cavity resonator described in the next section combines the symmetric response of the recessed transducer device with the reproducibility of the metal cavity design.

III. ETCHED CAVITY RESONATORS

As shown in Appendix I, the spurious peaks in the response of a metal cavity resonator are due to distortions of the transducer response which depends on the phase of the grating reflection coefficient. A modification of the metal cavity resonator structure that allows more flexibility in establishing the phase of the reflection coefficient at the cost of increased photolithographic resolution is shown in Fig. 3. In this structure double electrodes are employed to realize the transduction function with self aligned grooves to realize the reflection function. The relative position of the grooves now determines the sign of the reflection coefficient. The structure shown in Fig. 3a has grooves positioned between electrodes of alternate polarity resulting in a situation identical to the metal cavity resonator having an aluminum metallization. A resonator designed using this topology would exhibit a low frequency transmission peak and a high frequency transmission zero. The structure shown in Fig. 3b results in a situation that is identical to the metal cavity resonator having a gold metallization. The frequency response of this unit would be characterized by a low frequency transmission zero and a high frequency transmission peak.

Even more interesting is the configuration shown in Fig. 3c

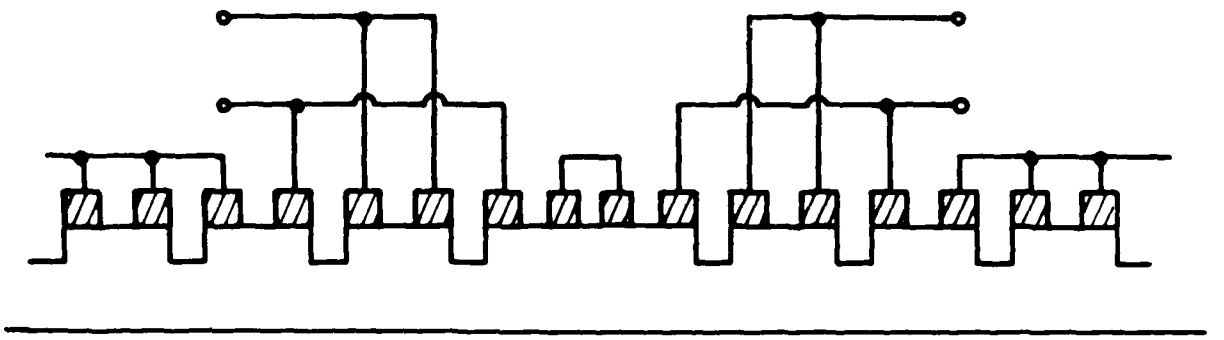

a.)

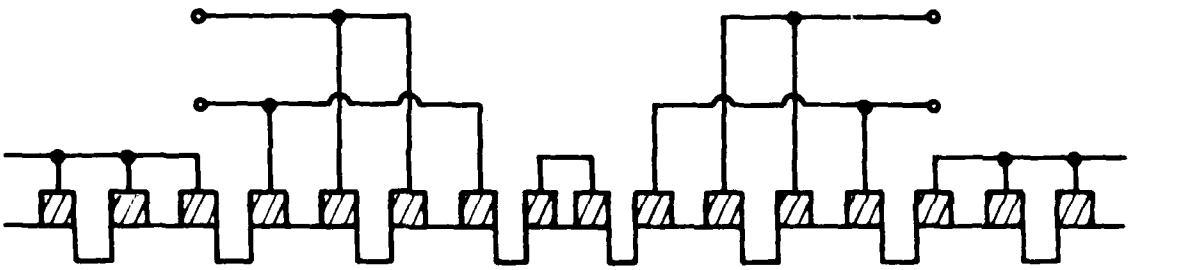

b.)

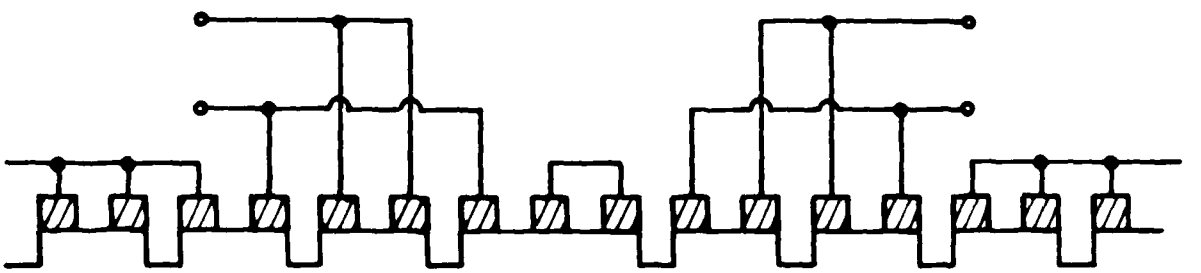

c.)

Figure 3. Etched cavity two-port resonator structures. a.) Structure having a high frequency transmission zero, b.) structure having a low frequency transmission zero, c.) structure having symmetric response.

in which both topologies are combined to give a symmetric response with reduced spuria. Since the reflection coefficient changes sign at the ends of the cavity, an additional 180° phase shift is added to the resonance condition that requires an integer number of quarter wavelengths in the cavity spacing. The non-synchronous phasing section is no longer needed for its phase shift, but can be retained to provide a smooth transition between gratings to minimize bulk mode scattering. Figure 4a shows the frequency response of a one pole resonator having the parameters listed in Table I that was calculated using an equivalent circuit technique. The real part of the input and output impedances in Fig. 4b show that the individual transducer transfer functions are not symmetric, although the device transfer function is highly symmetric, with good spurious attenuation.

Figure 5 illustrates the key steps in the fabrication of this device. After patterning the metallization, a second coat of photoresist is spun on and the second level pattern reproduced as in Fig. 5a. The slice is then etched to give a groove in the quartz that is self aligned to adjacent aluminum stripes as shown in Fig. 5b. Reactive ion etch techniques exhibit quartz etch rates that are 10 to 20 times the etch rate for aluminum [11], resulting in the desired self-aligned groove. Note that the alignment of the second level mask is non critical, in that the alignment tolerance

Table I

Device Parameters for Figure 4

Center frequency	215 MHz
Substrate material	ST Quartz
Grating length	200 wavelengths
Transducer length	40 wavelengths
Spacer length	1/2 wavelength (synchronous)
Beamwidth	100 wavelengths
Metal thickness	1000 A
Groove Depth	3000 A

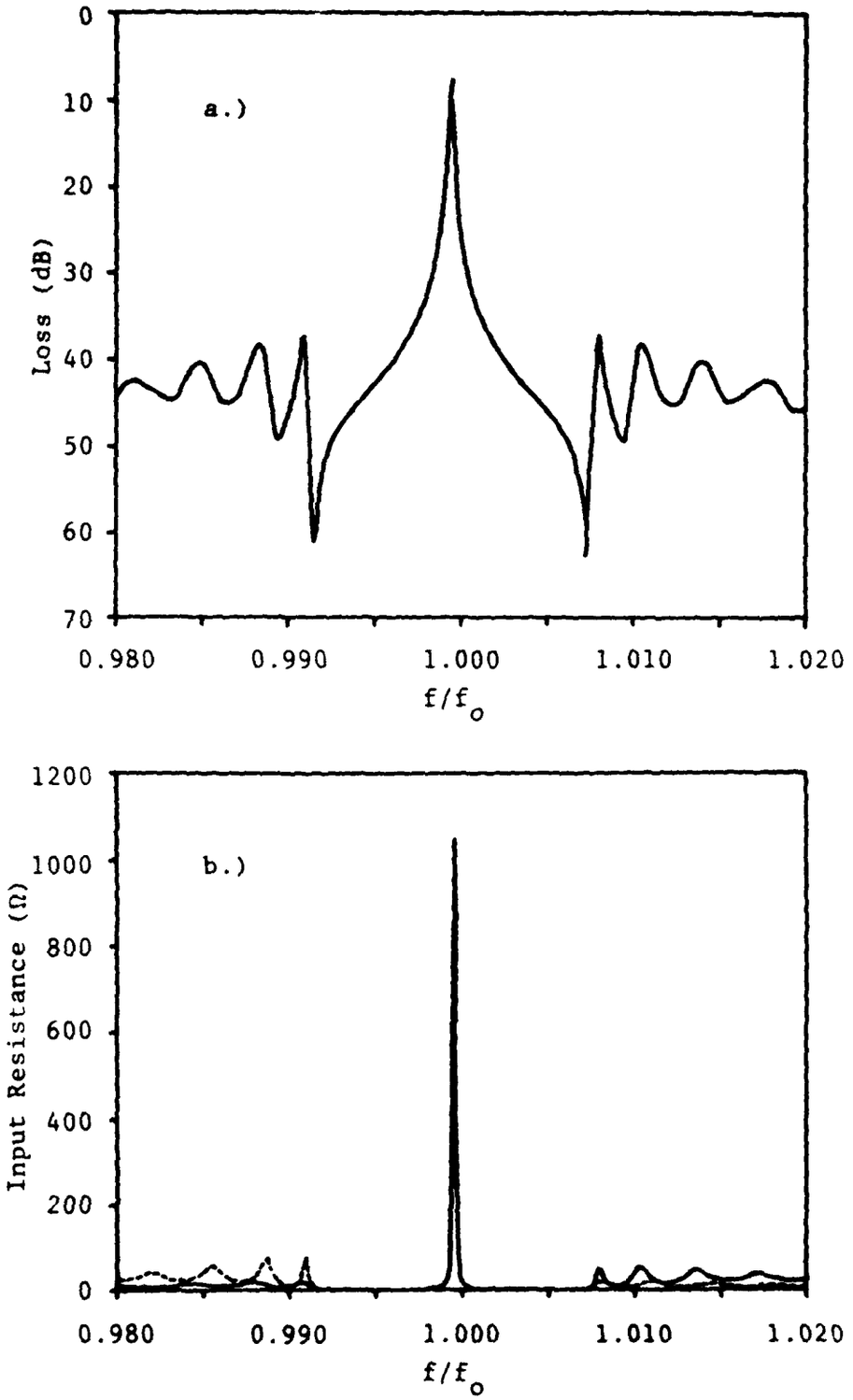

Figure 4. Etched cavity 2-port frequency response. a.) Insertion loss, b.) Input and output resistance.

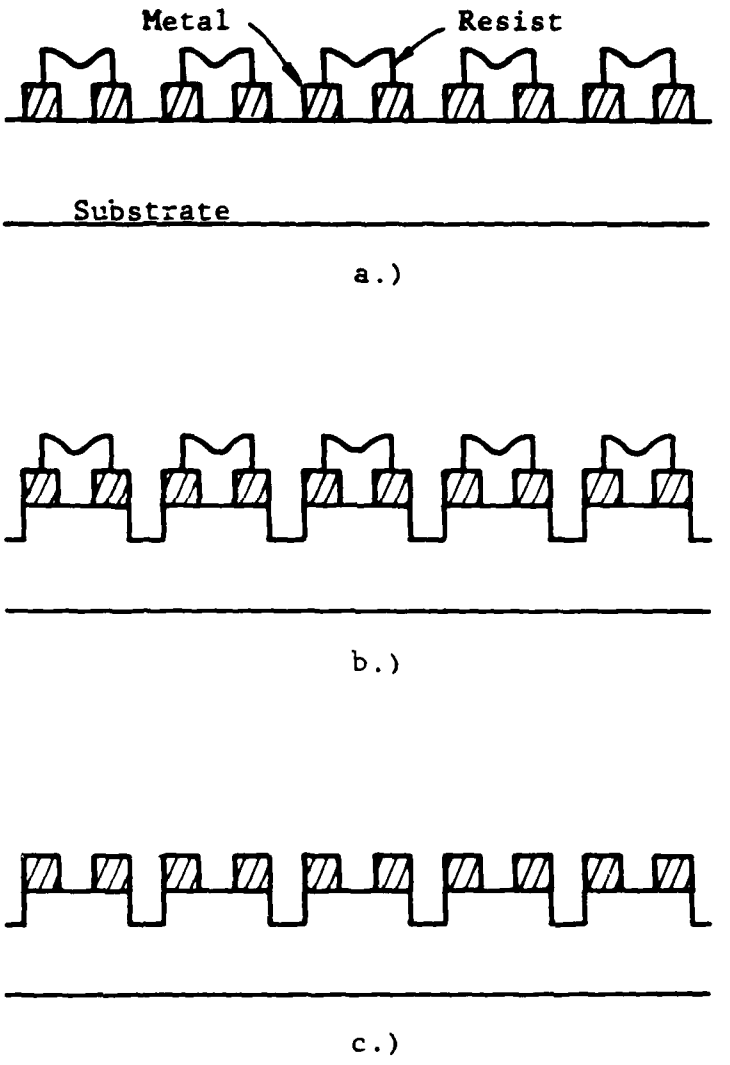

Figure 5. Etched cavity resonator fabrication steps. a.) Patterned 2nd level resist aligned on first level metallization, b.) self aligned quartz etch, c.) resist removed.

is established by the dimensions of the first level pattern. Finally the photoresist is stripped, giving the finished device topology shown in Fig. 5c.

Figure 6 shows one possible configuration of a two pole resonator using the self aligned process. The relative position of the grooves changes between transducer T_1 and the coupling grating, and between transducer T_2 and the right end grating to achieve complementary transducer transfer functions. The transfer function for this device is shown in Fig. 7a, with corresponding device parameters listed in Table II. Detailed response near the resonant frequency is shown in Fig. 7b.

In order to evaluate the etched cavity resonator concept, a mask set was designed and fabricated including two single pole, two port resonators having slightly different topologies, and two identical two pole resonator filter structures. A plot of the first level geometries is shown in Fig. 8. Resonator A incorporates a non-synchronous spacer to minimize possible bulk mode scattering. Resonator B does not have a spacer, but rather has two grounded stripes between transducers to provide isolation. The two identical two pole structures were positioned next to each other in order to evaluate device-to-device reproducibility. Each electrical port in the two pole devices is an individual two port, comprising two transducers that are separated by

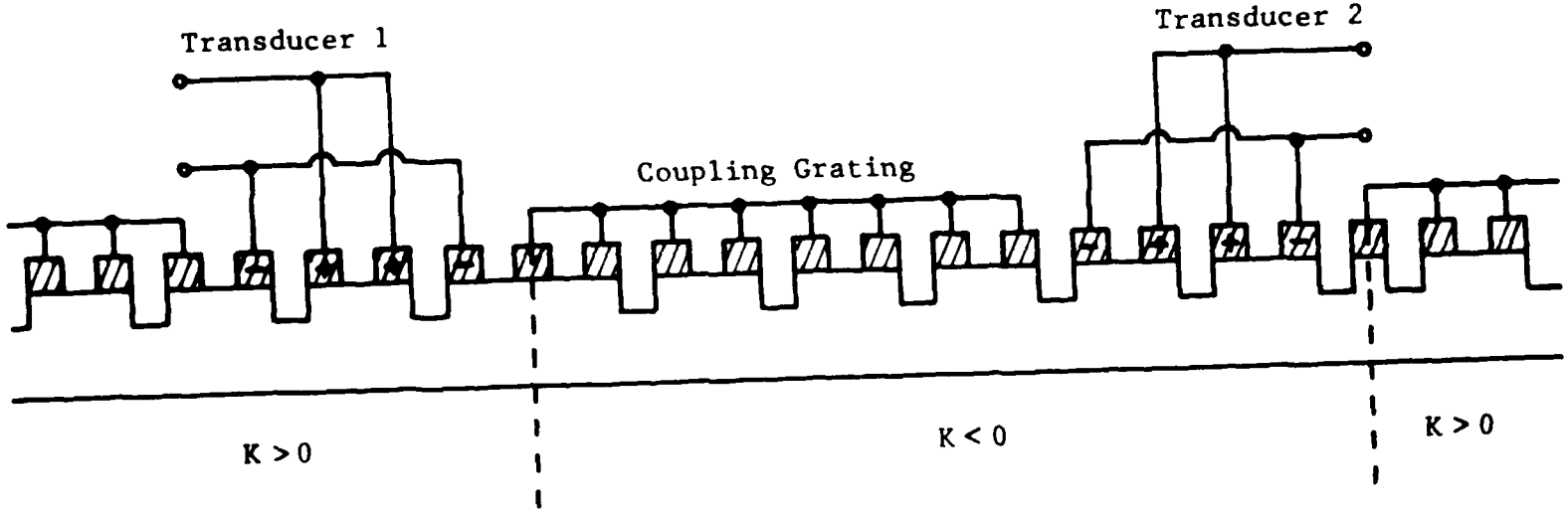

Figure 6. Etched cavity two pole resonator structure.

Table II

Device Parameters for Figure 7

Center frequency	215 MHz
Substrate material	ST Quartz
Grating length	200 wavelengths
Transducer length	40 wavelengths
Coupling grating length	100 wavelengths
Beamwidth	100 wavelengths
Metal thickness	1000 A
Groove Depth	3000 A

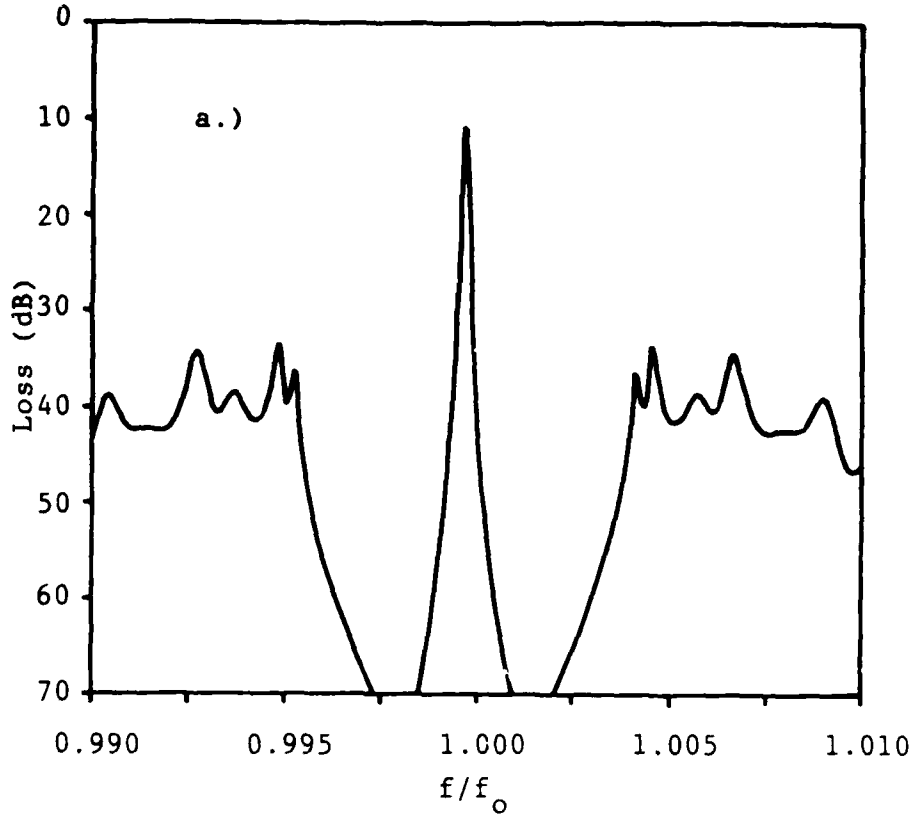

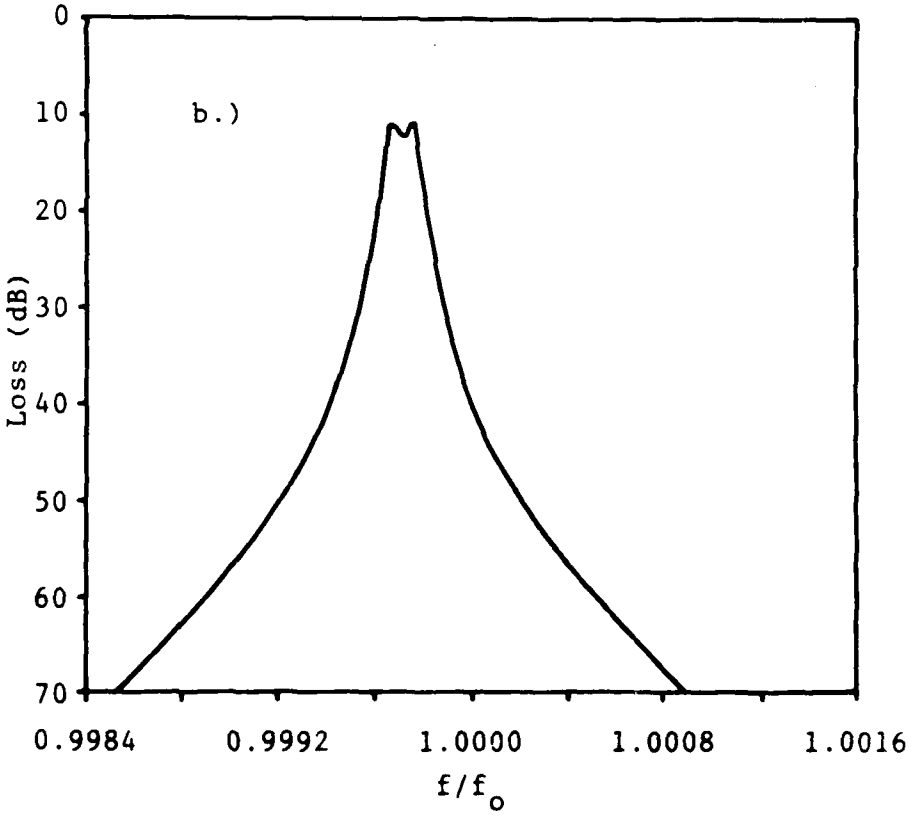

Figure 7. Etched cavity two pole frequency response. a.) Wide band, b.) detail.

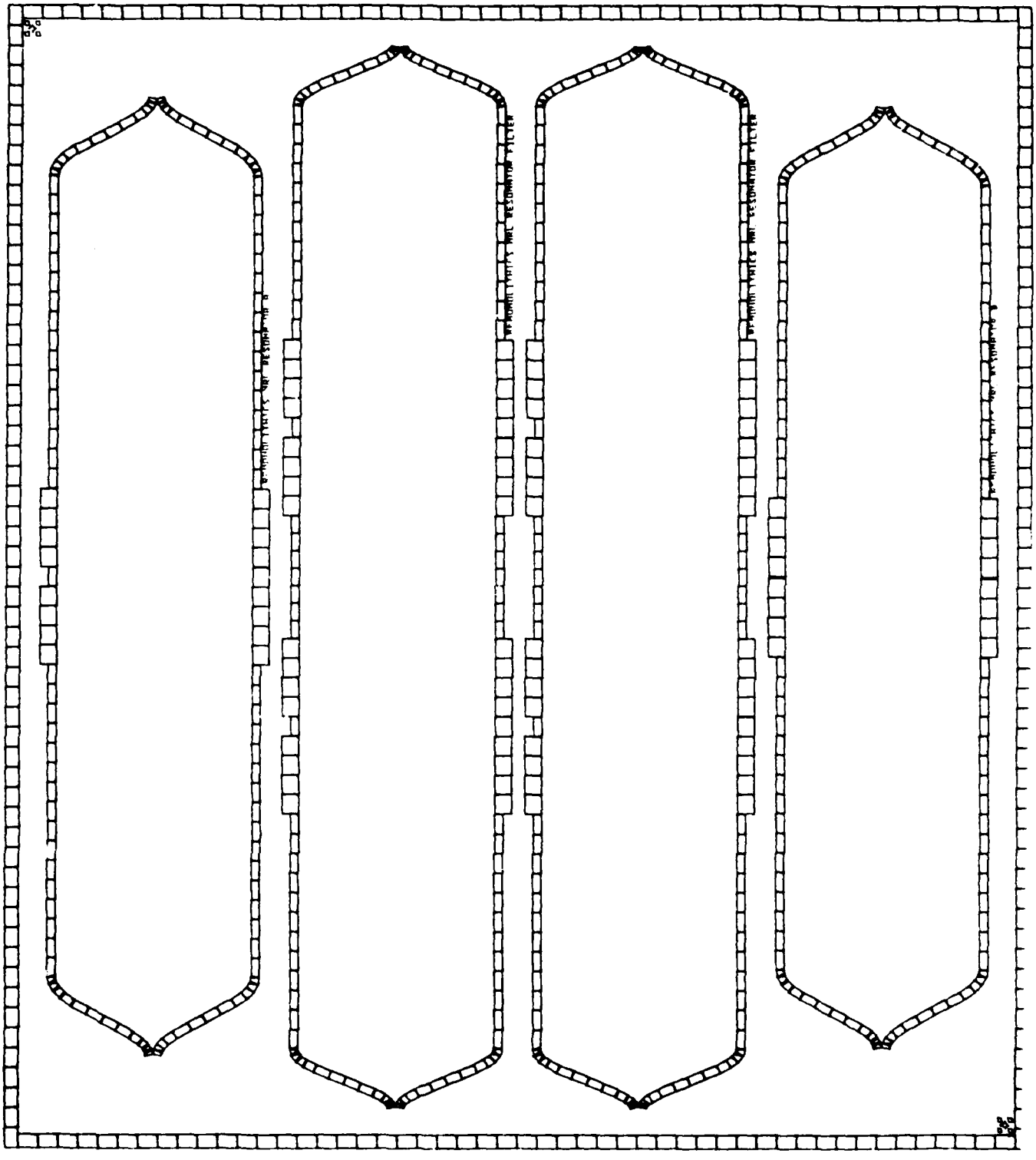

Figure 8. Test Bar check plot.

non-synchronous spacers. Besides minimizing bulk mode scattering, this allows individual evaluation of each section. The individual transducers must be interconnected in parallel to realize the complete two pole device.

The response of each of the devices in a 50 ohm system was calculated using an equivalent circuit analysis program. Figures 9 through 11 show calculated device response plots for the parameters listed in Table III. Inadvertantly, the effect of the overlap weighting employed to minimize the excitation of higher order transverse modes was not incorporated into the initial analyses. The weighting function is a modified cosine having an average value of approximately 0.45. The impedance levels in the experimental devices can be expected to be a factor of $1 / (.45)^2 = 4.9$ times larger than anticipated. Preliminary calculations for the device parameters listed in Table III predicted an equivalent series resistance of about 100 ohms in the single pole devices, resulting in approximately 6 dB insertion loss in a 50 ohm system. Inclusion of the effect of the weighting function in these devices raises the series resistance to about 500 ohms, and the insertion loss to about 16 dB, as shown in Figs. 9 through 11. Thus, the devices were designed on the basis of an optimistic prediction of their impedances, and the insertion loss predicted in the figures is substantially higher than initially anticipated.

Table III

Device Parameters for Figure 9

Center frequency	215 MHz
Substrate material	ST Quartz
Grating length	200 wavelengths
Transducer length	40 wavelengths
Spacer length	6 wavelengths
Beamwidth	100 wavelengths
Metal thickness	1000 A
Groove Depth	3000 A

Device Parameters for Figure 10

Center frequency	215 MHz
Substrate material	ST Quartz
Grating length	200 wavelengths
Transducer length	40 wavelengths
Spacer length	1/2 wavelength
Beamwidth	100 wavelengths
Metal thickness	1000 A
Groove Depth	3000 A

Device Parameters for Figure 11

Center frequency	215 MHz
Substrate material	ST Quartz
Grating length	150 wavelengths
Transducer length	40 wavelengths
Spacer length	6 wavelengths
Coupling grating length	100 wavelengths
Beamwidth	100 wavelengths
Metal thickness	1000 A
Groove Depth	3000 A

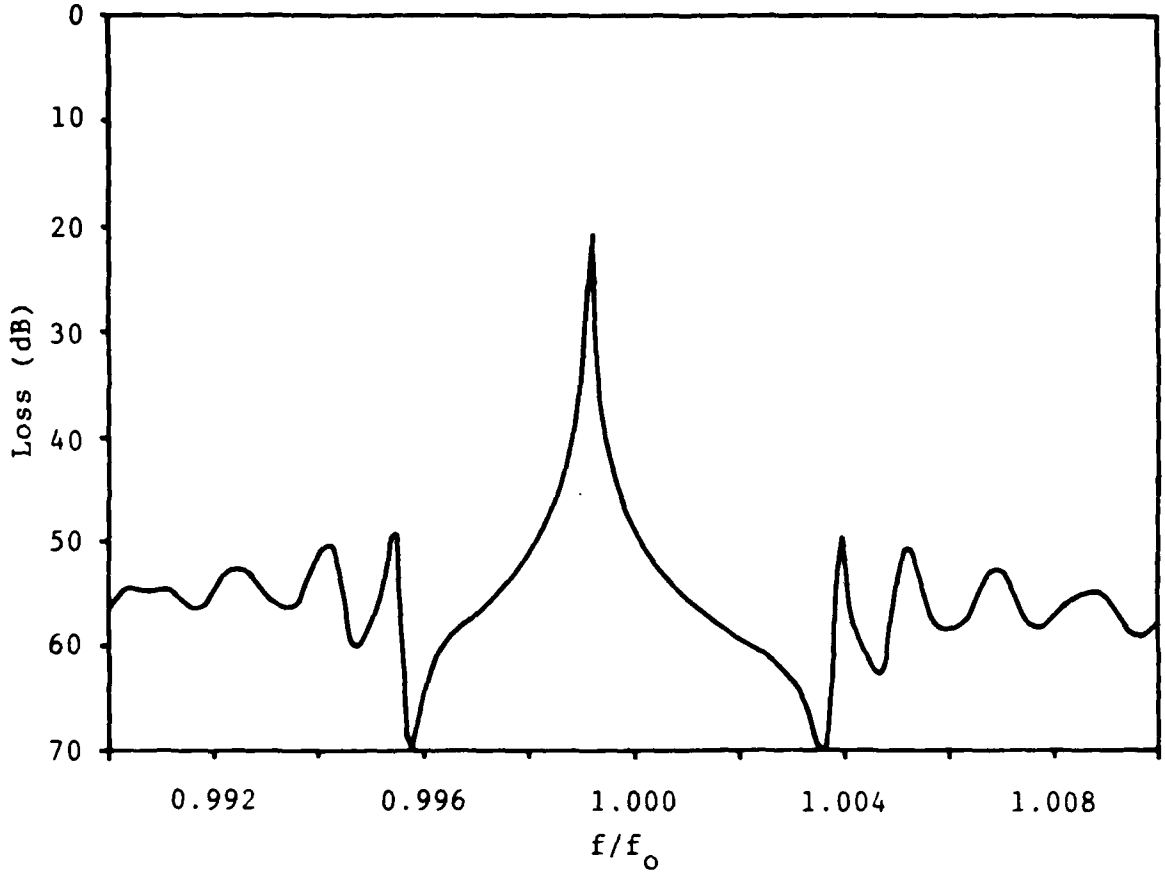

Figure 9. Test Bar resonator A frequency response.

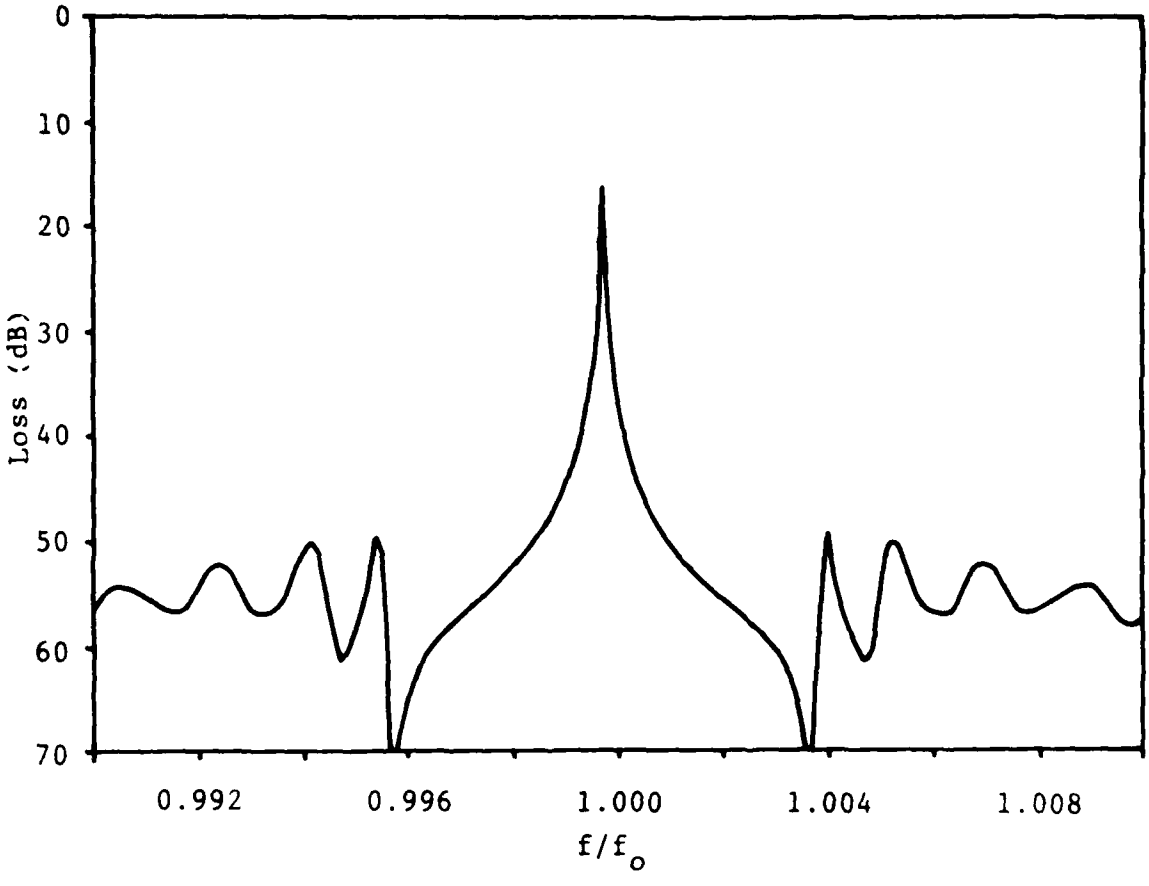

Figure 10. Test Bar resonator B frequency response.

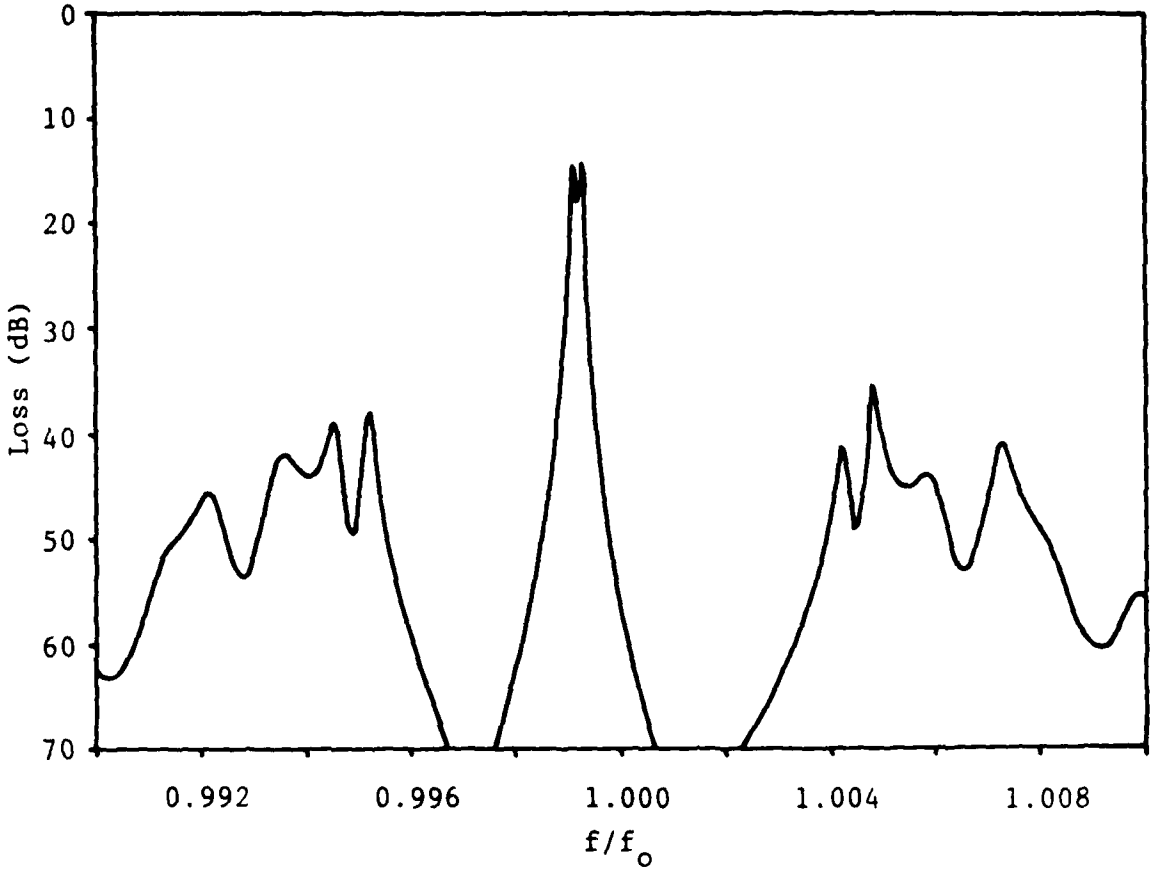

Figure 11. Test Bar two pole frequency response.

Device fabrication and test results are discussed in the following section.

IV. EXPERIMENTAL RESULTS

Initial Test Bar lots were fabricated with 2000A aluminum metallizations and were etched in a planar plasma etcher using CH_4 and O_2 [12]. Profilometer measurements indicated that a groove depth of about 1300A had been achieved, substantially less than the goal of 3000 to 4000A. Evaluation of the single pole test devices showed that the expected frequency response had been achieved, but that the most severe problem was multiple moding. Figures 12 and 13 show photographs of the frequency response of selected single moded devices from slices 2 and 3 of the first lot. The best performance was observed for device 8-3 of slice 2 which exhibited an insertion loss of 12 dB in a 50 ohm system, with an unloaded Q of 15000, about 60% of the material limit in air. The average response of the single moded devices from the first lot showed an insertion loss of 16 dB with an unloaded Q of 9000, compared to predicted values of approximately 12dB and 24000 respectively.

The groove reflection coefficient was measured experimentally by measuring the grating transmission coefficient in the coupler section of a two pole test device. Reflector arrays at the ends of the structure were damped with a silicone rubber compound. The measured response is shown in Fig. 14 which shows a stop band attenuation of about 20 dB. Interpretation of the experimental data is somewhat

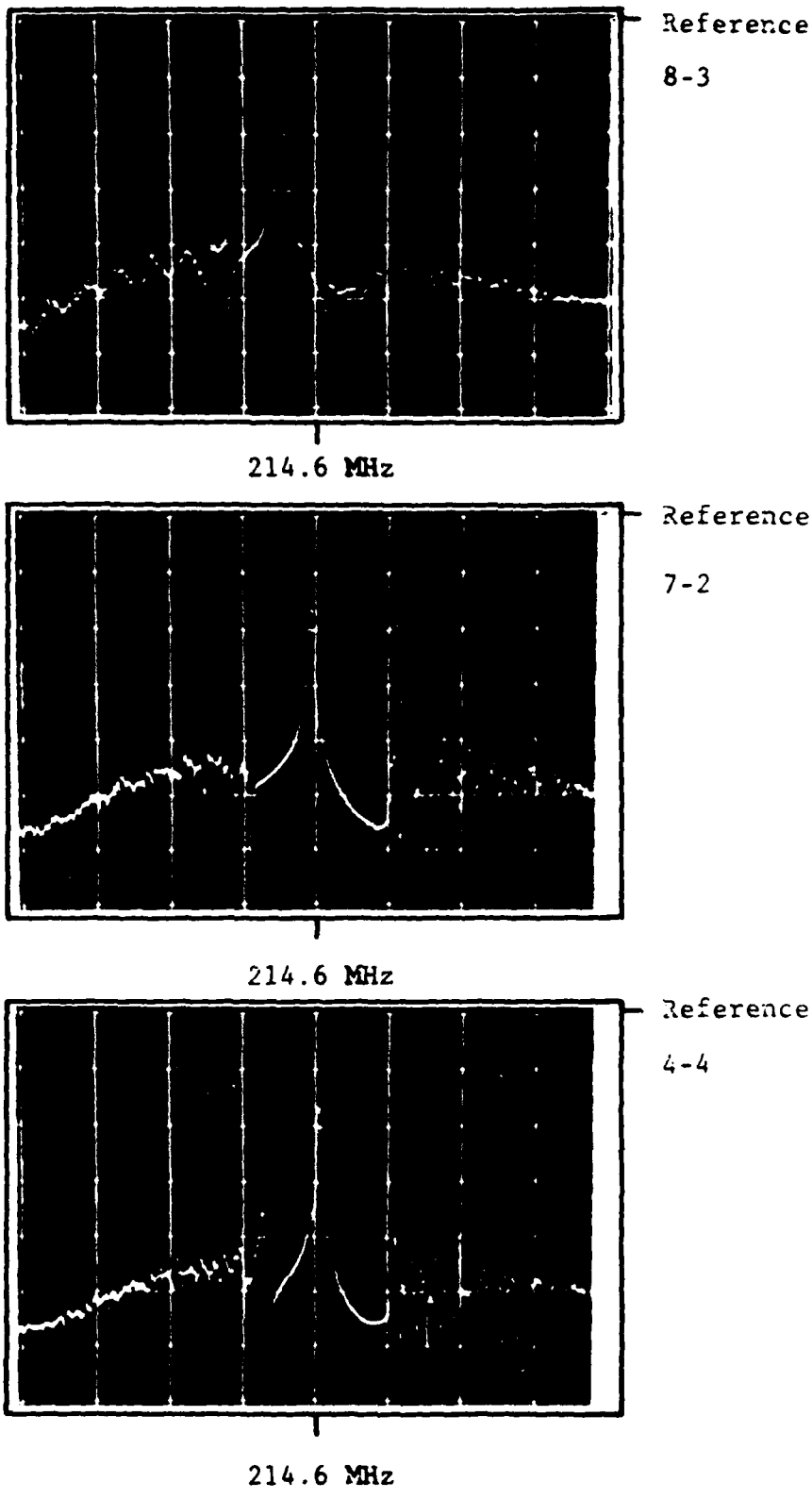

Figure 12. Test Bar Slice 2 1-pole experimental response. Vertical 10 dB/div, horizontal 1 MHz/div.

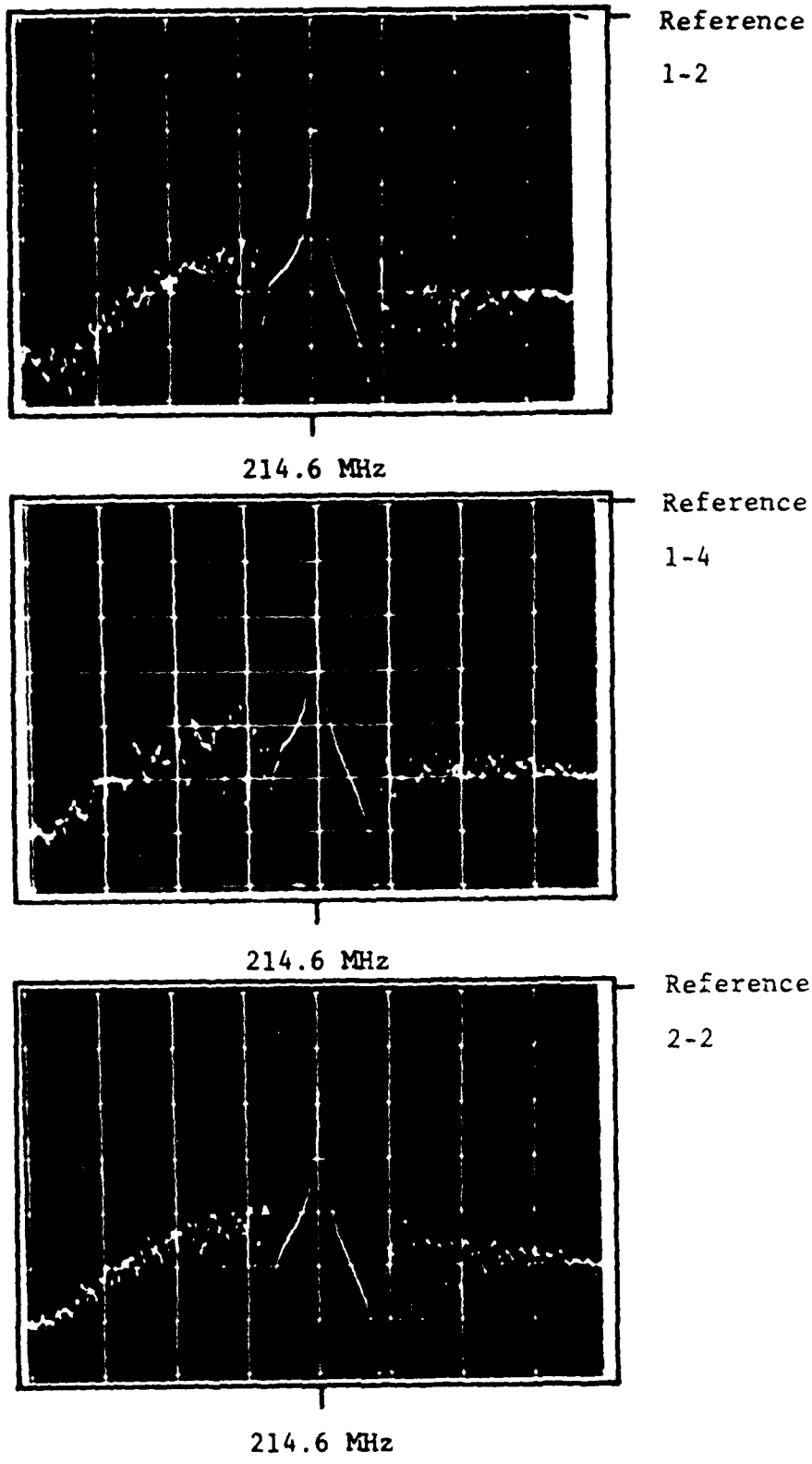

Figure 13. Test Bar Slice 3 1-pole experimental response. Vertical 10 dB/div, horizontal 1 MHz/div.

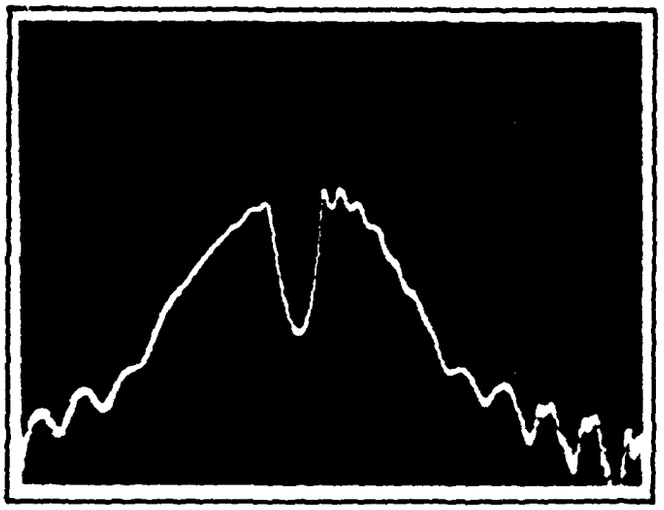

Figure 14. Grating transmission response. Vertical 10 dB/div, horizontal 2.65 MHz/div.

complicated by the fact that the transducers are incorporated within the grating. Employing the expression for the transducer transfer function given in equation (12) of Appendix I and using the expression for the grating reflection coefficient in equation (1) of that appendix, the transfer function of the experimental device at the center frequency normalized to the response of two non-reflecting transducers can be shown to be:

$$T = 2\,[1 - \mathrm{sech}(KL_T)]\,[1 - \tanh(KL_R)] \,/\, (KL_T)^2 \qquad (1)$$

Solving (1) for K results in the experimental value K = 0.021. The first order reflection coefficient for a groove in ST quartz is approximately

$$k = 0.5\,(h \,/\, \lambda)\,\sin(2\,\pi\,\, d \,/\, \lambda) \qquad (2)$$

where d is the dimension of the groove in the propagation direction. For 1/8 wavelength grooves 1300A deep, this gives a value of K = 2k = .64%, less than one third of the value observed. Although the groove depth is uncertain by as much as 50%, the value of K is substantially larger than the worst case first order term. This suggests that the shallow grooves have steep walls, thereby increasing the contribution of the stored energy (second order) terms. Figure 15 shows a plot of K versus groove to space ratio for various edge profiles as specified by the edge to space ratio [13]. Note

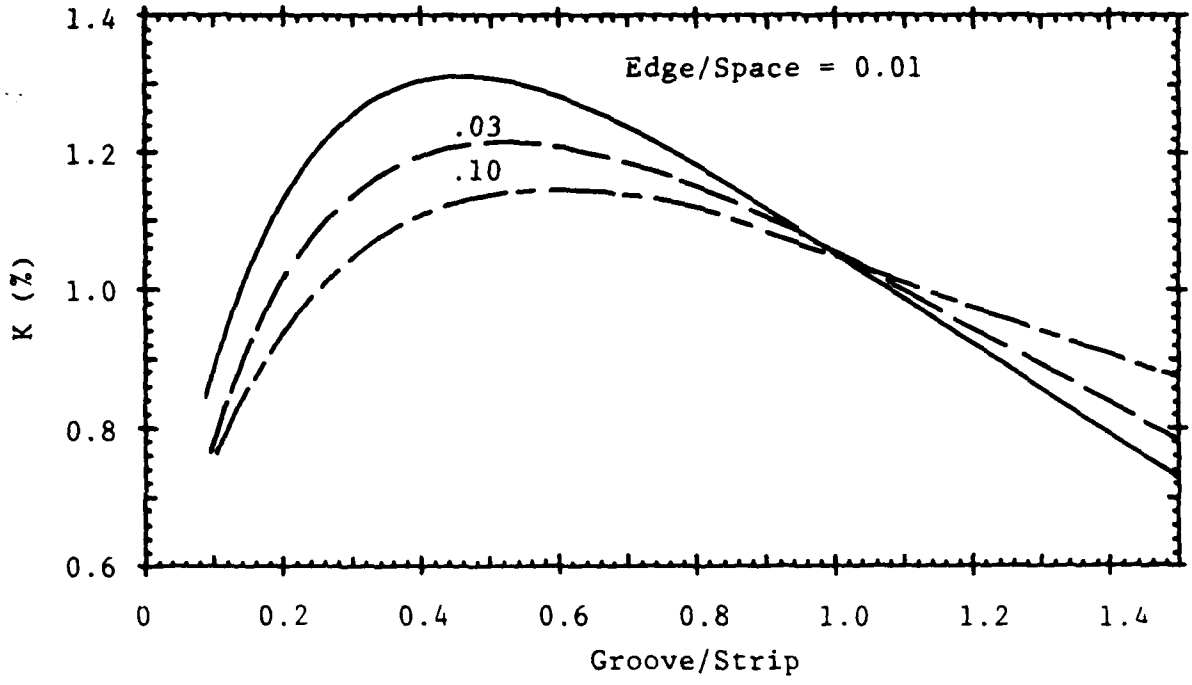

Figure 15. K versus Groove/Space ratio with Edge/Space ratio as a parameter.

that K is a strong function of edge to space ratio for steep walled grooves, leading to a sensitivity to groove profile that can be expected to cause variations in K and in the SAW velocity.

From these results it was concluded that device performance was limited by an anomolous loss mechanism and/or by nonuniformities in groove depth or profile. Subsequent examination of these initial devices in an SEM [14] showed groove depths of about 1400A and degraded surface quality both within the grooves and, in some cases, beneath the second level resist layer as shown in Fig. 16. The former condition has been attributed to polymer formation during the etch caused by excessive gas pressure and low plasma power densities [15]. The measured groove depth is taken to the top of the "pillars" caused by polymer formation, the effective groove depth is undoubtedly larger than this value. The polymer layer itself can be expected to be extremely lossy, however, it was in all likelihood removed by the intense UV cleaning employed before device testing [16]. The surface irregularities etched into the quartz will also cause increased propagation loss due to nonsynchronous scattering [17].

The latter condition is caused by polymerization of the second level photoresist that renders it insoluble in common solvents. However, this layer can be removed by ashing in an

Figure 16. SEM of plasma etched device. Magnification 10 kX.

oxygen plasma. Either of these conditions result in additional loss that can be expected to degrade device performance.

The strong dependence of K on groove profile suggests that minor variations in that parameter may be responsible for the multiple moding observed by causing variations in velocity across the device. Several additional slices were fabricated with longer etch times in an attempt to achieve deeper grooves with shallower walls. No improvement in device response was achieved using the planar plasma etcher. However, polymer formation inhibits quartz etching [15], and it is likely that the longer etch times did not result in substantially deeper grooves.

Several test slices were subsequently sent to Drytek, Inc. [18] in order to evaluate the application of reactive ion etch (RIE) techniques. Two of the test slices were metal cavity resonators designed to operate at 303.5 MHz with a nominal 2500A aluminum metalization. In this case the devices were to be fabricated with 1000A of aluminum and the quartz etched to a depth of 1500A. SEM analysis of the completed slices indicated that the quartz had been etched to 1000A with steep walls, and that polymer formation had occurred. Device evaluation showed that the desired K had been achieved, probably due to the quartz etch profile, however the device insertion loss and unloaded Q were

substantially degraded, compared to the metal cavity units. Average device parameters are listed in Table IV.

The other two slices processed at Drytek were Test Bars that had been completed through second level patterning. In order to minimize the effect of photoresist polymerization, the second level pattern was etched in a 2000A chrome film that can be easily removed without disturbing the underlying aluminum pattern. Device evaluation showed that K had more than doubled, but that the device response had not improved. Figure 17 shows the response of one of the few devices that exhibited single moded response. Figure 18 shows an SEM photograph of the surface of one of the test devices from which all metal has been removed. The apparent etch depth is 5000A, but the vertical walls and substantial polymer formation have unquestionably degraded device response.

In a final attempt to achieve reasonable and reproducible device response, the self aligned process was altered to permit ion milling of the quartz grooves. Ion milling is a well developed process in which etch contour can be controlled [19], however, there is little etch selectivity between aluminum and quartz. Figure 19 shows the key steps in the modified process. The main difference is that the first level photoresist is not removed before the second level resist is applied and patterned. Thus the first level resist acts as an etch mask to prevent erosion of the

Table IV

303.5 MHz Resonator RIE Evaluation Data

Parameter	Metal Cavity	RIE
Metal thickness	2500A	1000A
Etch depth	-	1000A
Insertion loss	4dB	7.9dB
Unloaded Q	20300	12100

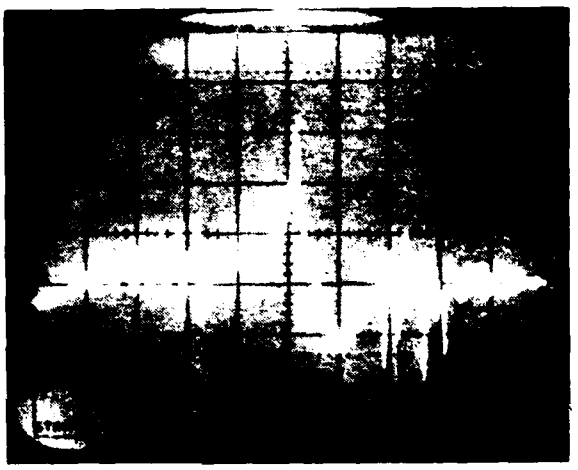

Figure 17. Response of Drytek RIE device. Vertical 10 dB/div, horizontal 1 MHz/div.

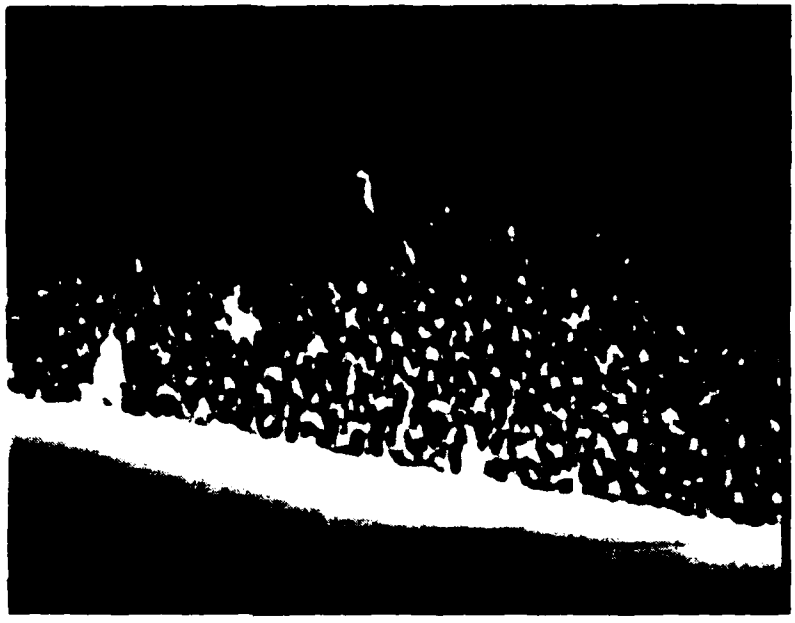

Figure 18. SEM of Drytek RIE device. Magnification 30 kX.

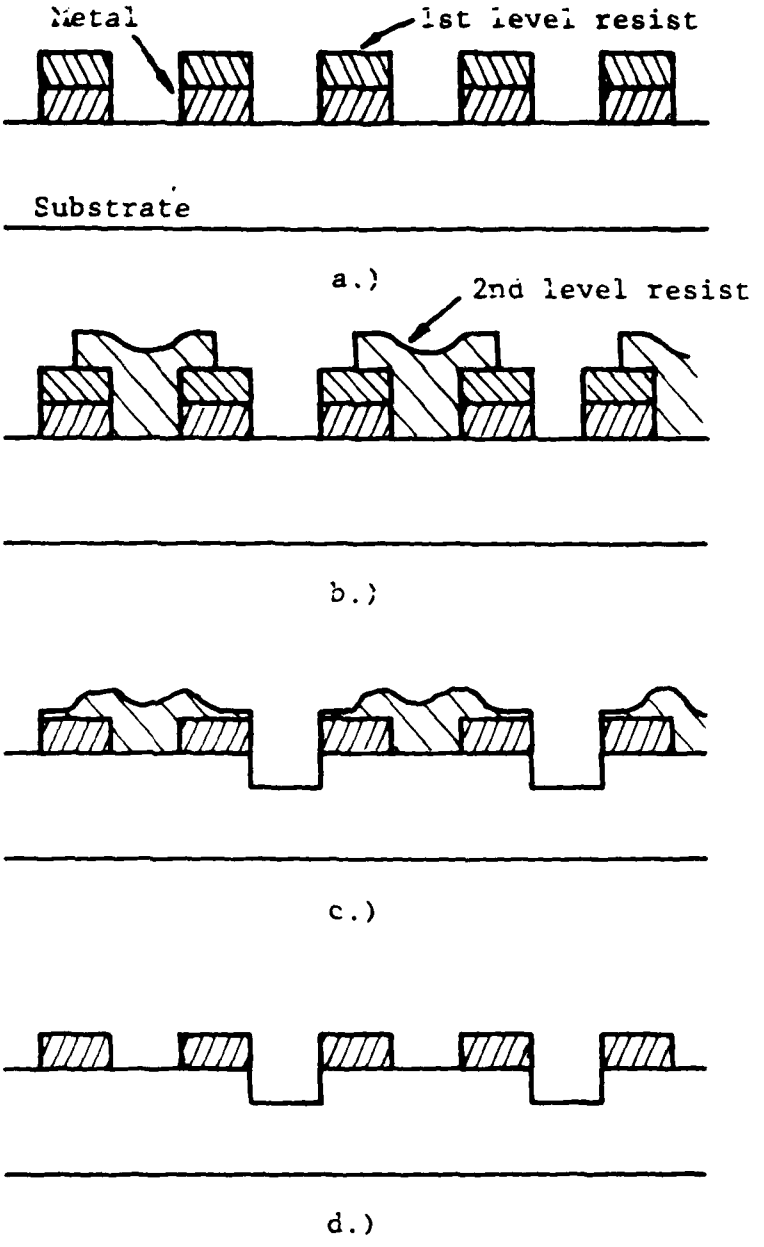

Figure 19. Ion milled etched cavity process steps. a.) First level metal patterned, resist not removed, b.) second level resist patterned, c.) after ion milling, d.) all resist removed.

aluminum pattern during groove formation. Any resist remaining after the milling operation is polymerized and must be removed in an oxygen plasma.

Evaluation of device response was encouraging. Although the Q is still lower than expected, the devices were predominately single moded. In addition, the standard deviation in center frequency was observed to be less than 200 ppm, a substantial improvement over earlier results and indicative of improved control of device topology. Typical device response photographs appear in Fig. 20. The grating transmission experiment was repeated and the results shown in Fig. 21 yield a value of K = 0.018, slightly smaller than in the initial experiments.

Figure 22 shows an SEM photograph of one of the ion milled devices. Although there is evidence of redeposited material in the grooves, the average groove depth is approximately 3300A, and the groove profile is substantially shallower than observed in previous attempts. In this case the first order groove reflection coefficient gives K = 1.6%, in reasonable agreement with observation.

Two of the two pole filter test structures were found to exhibit reasonable response, albeit at high insertion loss. Figure 23 shows the frequency response of these devices obtained using an RF probe at slice level. Because only a

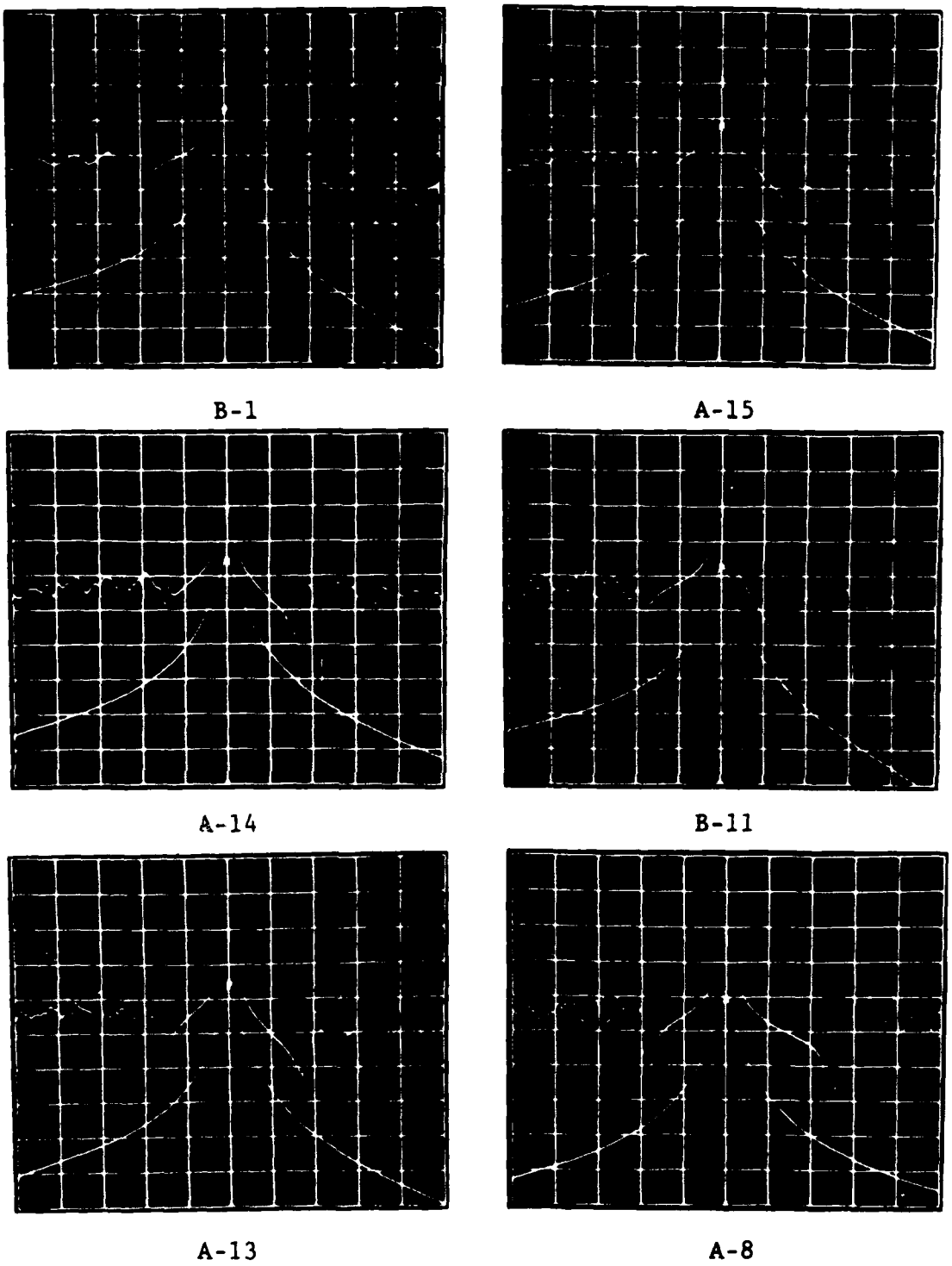

Figure 20. Ion milled 1-pole experimental response. Wide band: Vert. 0.5 MHz/div, horiz. 10 dB/div. Narrow band: Vert. 0.1 MHz/div, horiz. 5 dB/div.

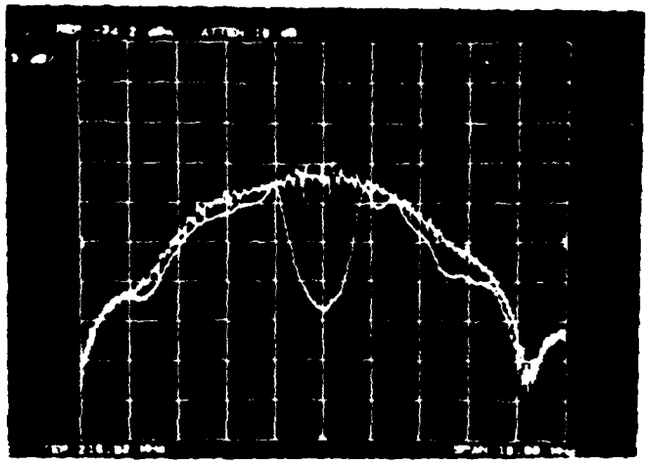

Figure 21. Ion milled grating transmission response. Vertical 5 dB/div, horizontal 1 MHz/div.

Figure 22. SEM of ion milled device. Magnification 10 kX.

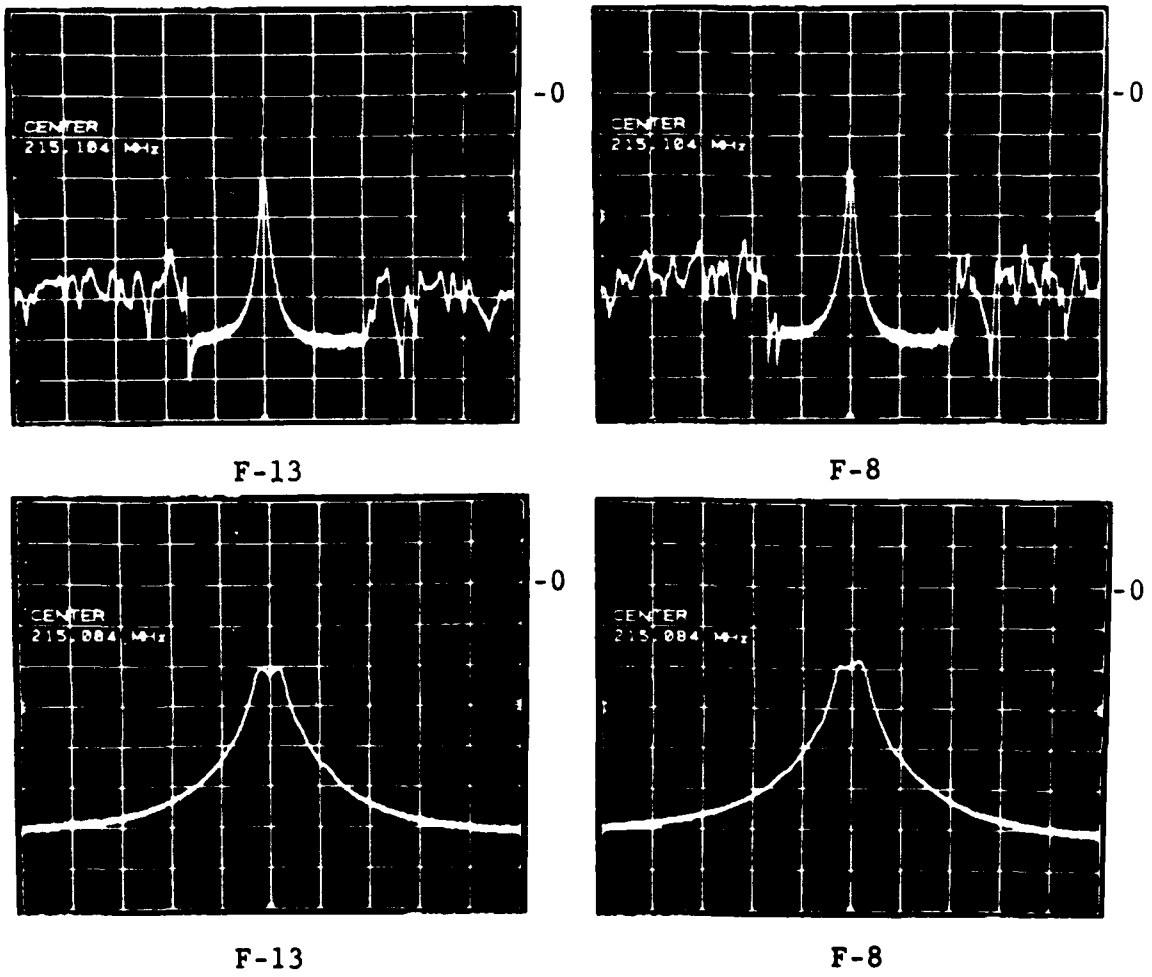

Figure 23. Ion milled 2-pole response. Upper: vertical 10 dB/div, horizontal 0.5 MHz/div. Lower: vertical 10 dB/div, horizontal 0.1 MHz/div.

limited number of probes were available, these response photographs were obtained while driving only one of the two transducers that comprise each section. Thus, it can reasonably be expected that the insertion loss of the complete structure would be about 6 dB lower than shown.

Although better reproducibility has been achieved using ion milling, the high insertion loss and low Q are still troublesome. Recommendations for further work to improve device response are discussed in the next section.

V. CONCLUSIONS

The experimental results from the first lot of Test Bar devices showed that, although the expected frequency response function was achieved, the most serious problem with the etched cavity resonator structure was the poor uniformity in K, the groove reflection coefficient, and excess propagation loss that is suspected as being due to the poor surface quality in the grooves. Subsequent development of an ion milling process resulted in better uniformity, but the loss did not improve, probably due to the redeposited material observed within the grooves. A substantial process development remains if the etched cavity structure is to be effectively utilized in realizing SAW resonator elements for multi pole filters.

The groove depths achieved during this program are substantially below the limits described in the literature for which bulk mode radiation losses become appreciable [20]. However, the published experimental limits were established for grooves having approximately unity groove to space ratio, for which the stored energy contribution to K is small (see Fig. 15.) The small groove to space ratios employed in the etched cavity structure result in strong stored energy contributions and may also be reponsible for enhanced bulk mode radiation, resulting in lower device Q. An analysis of

this problem is beyond the scope of the present work, but should be pursued since it may constitute an intrinsic limitation to the etched cavity resonator structure.

Note that, although the frequency response function of the etched cavity structure is symmetric, the individual transducer transfer functions are non-symmetric, and the transducers are not peak positioned. This situation is due to the fact that the groove reflection coefficient is imaginary when referenced to the center of transduction which is located in the center of a gap between electrodes of the same polarity [21]. Were it feasible to recess one of the transducer stripes within a groove, the additional 90^{o} phase shift would result in synchronization of reflection and transduction functions, thereby realizing peak coupling to the cavity standing wave. Of course, such a condition cannot be realized with a self aligned process.

Figure 24 shows the topology of a structure that does not require etched grooves, but results in peak positioned transducers and a symmetric frequency response. Rather, a double level metallization is employed to synchronize reflection and transduction functions. This technique has been employed recently to evaluate a unique low loss filter concept based on the control of transducer internal reflections [22]. A reprint of the paper describing the theory and experiments that was delivered at the 1982 IEEE

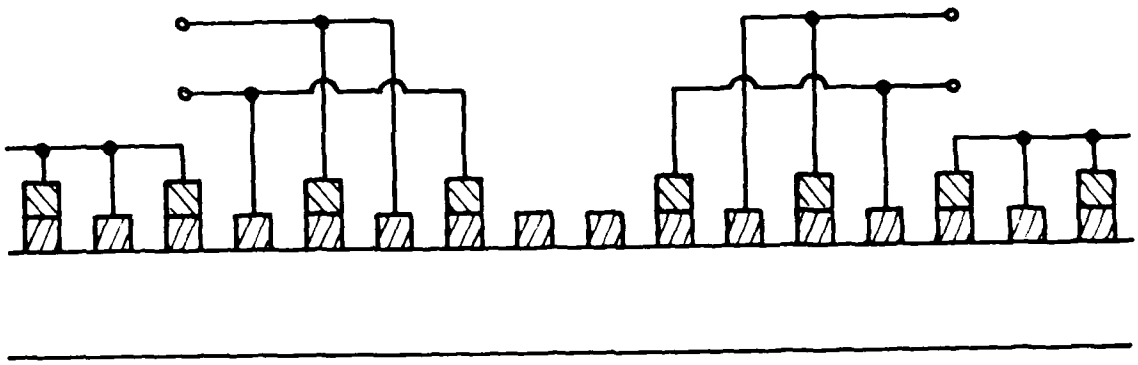

Figure 24. Double level metal resonator structure.

Ultrasonics Symposium is included in Appendix II. Figure 25 shows the key fabrication steps involved. The first level pattern delineating all critical geometries is first etched into the double level metallization as shown in Fig. 25a. After stripping the first level resist, a new layer of resist is applied and the second level pattern is exposed and developed, resulting in the structure shown in Fig. 25b. Note that the process is again self aligned, but requires that the two metals employed be compatible for selective etching, or that a thin barrier metal film be deposited between identical metal layers. The final pattern is shown in Fig. 25c.

Based on RF Monolithics' experience in fabricating multilevel low loss SAW filters, and on the preliminary results discussed in Appendix II, it is anticipated that this double level metal approach will be considerably more reproducible than the etched cavity approach, and will lead to high performance SAW resonator elements for multipole filter applications.

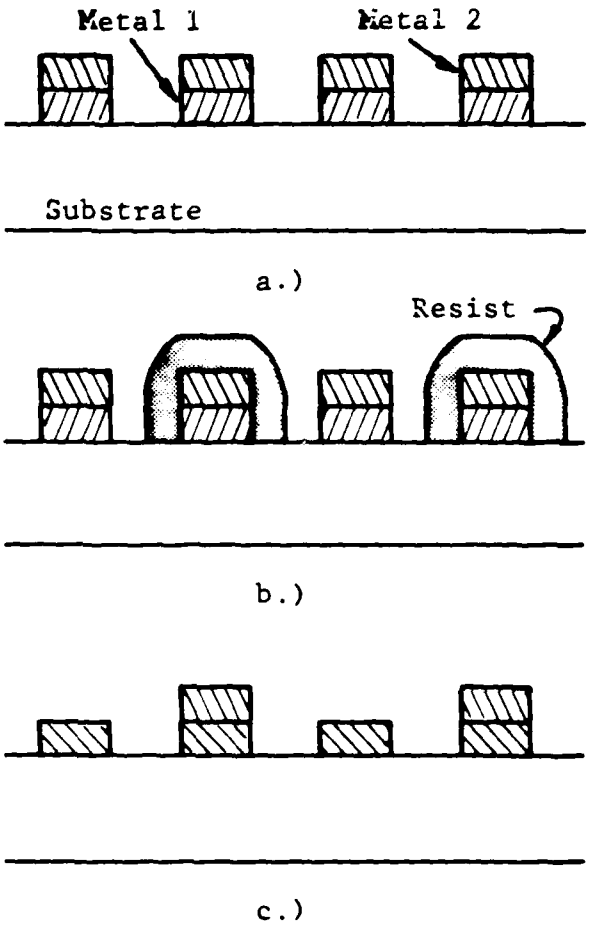

Figure 25. Double level metal fabrication steps.
a.) First level patterned in both metallization layers, b.) second level resist patterned, c.) top level metallization etched and resist removed.

VI. REFERENCES

[1] W. J. Tanski, 'Surface Acoustic Wave Resonators on Quartz,' IEEE Trans. Sonics and Ultrasonics, SU-26, No. 2, pp. 93-104, March 1979.

[2] W. J. Tanski, 'GHz SAW Resonators,' Proc. 1979 Ultrasonics Symposium, IEEE Catalog No. 79CH1482, pp. 815-823.

[3] W. J. Tanski, 'High Performance SAW Resonator Filters for Satellite Use,' Proc. 1980 Ultrasonics Symposium, IEEE Catalog No. 80CH1602, pp. 148-152.

[4] W. J. Tanski, 'Elements of SAW Resonator Fabrication and Performance,' Proc. 35th Ann. Freq. Control Symposium, Ft. Monmouth N.J., pp. 388-394.

[5] W. J. Tanski, 'Multipole SAW Resonator Filters,' Proc. 36th Ann. Freq. Control Symposium, Ft. Monmouth N.J., pp. 400-404.

[6] W. J. Tanski, 'Multipole SAW Resonator Filters: Elements of Design and Fabrication,' Proc. 1981 Ultrasonics Symposium, IEEE Catalog No. 81CH1689, pp. 100-104.

[7] P. S. Cross, W. R. Shreve and T. S. Tan, 'Synchronous IDT SAW Resonators with Q Above 10,000,' Proc. 1979 Ultrasonics Symposium, IEEE Catalog No. 79CH1482, pp. 824-829.

[8] J. Wise, J. Schoenwald and E. Staples, 'Impedance Characterization and Design of 2-pole Hybrid SAW Resonator Filters,' Proc. 1980 Ultrasonics Symposium, IEEE Catalog No. 80CH1602, pp. 200-203.

[9] H. A. Haus, 'Bulk Scattering Loss of SAW Grating Cascades,' IEEE Trans. Sonics and Ultrasonics, SU-24, No. 4, pp. 259-267, July 1977.

[10] W. E. Bulst and E. Willibald, 'Ultrareproducible SAW Resonator Production,' Proc. 36th A.. Freq. Control Symposium, Ft. Monmouth N.J., pp. 442-452.

[11] T. Uno and H. Jumonji, 'Optimization of Quartz SAW Resonator Structure with Groove Gratings,' IEEE Trans. Sonics and Ultrasonics, SU-29, No. 6, pp. 299-310, November 1982.

[12] S. Elliot, M. Mierzwinski and P. Planting, 'The Production of Surface Acoustic Wave Resonators,' Proc. 1981 Ultrasonics Symposium, IEEE Catalog No. 81CH1689, pp. 89-93.

[13] P. V. Wright, Ph.D. Dissertation, Massachusetts Institute of Technology, April 1981.

[14] The SEM micrographs were obtained several months after initial device testing.

[15] A. D. Weiss, 'Plasma Etching of Oxides and Nitrides,' Semiconductor International, pp. 56-62, February 1983.

[16] J. R. Vig, 'UV/Ozone Cleaning of Surfaces: A Review,' in Surface Contamination: Genesis, Detection and Control, K. L. Mittal ed., Vol. 1, pp. 235-254, Plenum Press, New York, 1979.

[17] R. G. Steg and P. G. Klemens, 'Scattering of Rayleigh Waves by Surface Irregularities,' Phys. Rev. Letters, 24, No. 8, pp. 381-383, February 1970.

[18] Drytek, 220 Ballardvale St., Wilmington MA 01887.

[19] L. F. Johnson, 'Evolution of Grating Profiles Under Ion-beam Erosion, ' Applied Optics, 18, No. 15, pp. 2559-2574, August 1979.

[20] R. C. M. Li, J. A. Alusow and R. C. Williamson, 'Experimental Exploration of the Limits of Achievable Q of Grooved Surface-Wave Resonators,' Proc. 1975 Ultrasonics Symposium, IEEE Catalog No. 75CH0994-4SU, pp. 279-283.

[21] W. H. Haydl, P. Hiesinger, R. S. Smith, B. Discher and K. Heber, 'Design of Quartz and Lithium Niobate SAW Resonators Using Aluminum Metallization,' Proc. 30th Ann. Freq. Control Symposium, Ft. Monmouth N.J., pp. 346-357.

[22] C. S. Hartmann, P. V. Wright, R. J. Kansy and E. M. Garber, 'An Analysis of SAW Interdigital Transducers with Internal Reflections and the Application to the Design of Single-Phase Unidirectional Transducers,' Proc. 1982 Ultrasonics Symposium, IEEE Catalog No. 82CH1623, pp. 40-45.

APPENDIX I

Spurious Modes in SAW Resonators

In this Appendix we first consider the excitation of the resonant modes of the acoustic cavity formed by two grating reflectors. The structure of interest is shown in Fig. 1 which demonstrates the conventions to be used herein. The grating period is taken to be p = 2d where d is the center to center spacing between individual reflecting elements. The length of each grating is $L_R = N\ p$, where N is an integer, while the grating spacing is L_S which is an arbitrary length. Employing the coupling of modes formalism [1], the reflection coefficient of a single grating, referred to the edge of the first reflecting element, is given by

$$R = [K \sinh(GL_R)]/ [G \cosh(GL_R) + j\ D \sinh(GL_R)] \qquad (1)$$

where K is the reflection coefficient of the reflecting elements per wavelength, D is the detuning

$$D = 2\ \pi\ (\ 1/p - 1/\lambda\ ) \qquad (2)$$

and $G^2 = K^2 - D^2$. Equation (1) has particularly simple forms for the following special cases:

a) $G = K,\ D = 0$ (3)

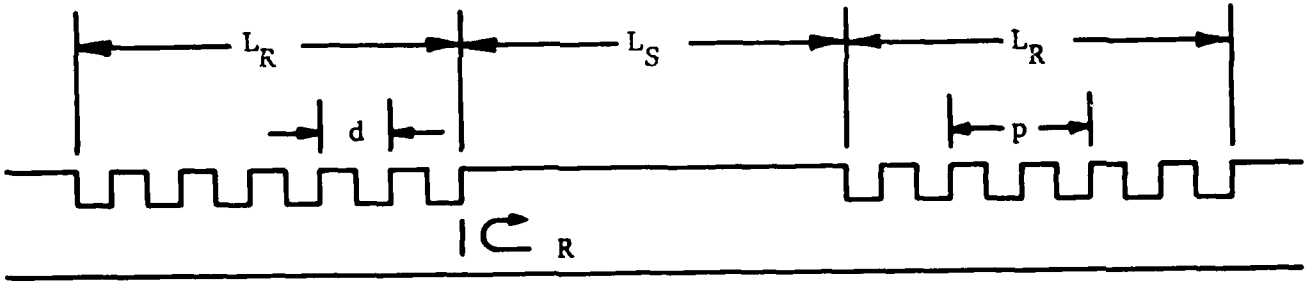

Figure 1. The basic SAW resonator structure.

$$|R| = \tanh(KL_R)$$

$$\phi = 0$$

b) $G = 0,\ D = K$ (4)

$$|R| = [\ 1 + (1/KL_R)^2\ ]^{-1/2}$$

$$\phi = \tan^{-1}(KL_R)$$

c) $G\,L_R = j\,\pi/2,\ D = K\,[\ 1 + (\ \pi\ /\ 2\,KL_R)^2\ ]^{1/2}$ (5)

$$|R| = [\ 1 + (\ /2KL_R)^2\ ]^{-1/2}$$

$$\phi = \pi\ /\ 2$$

d) $G\,L_R = j\,\pi\ ,\ D = K\,[\ 1 + (\ \pi/KL_R)^2\ ]^{1/2}$ (6)

$$|R| = 0$$

$$\phi = \pi$$

Case a) corresponds to the grating stop band center frequency, while d) corresponds to the first zero in the grating reflection coefficient.

We first consider the case in which non reflecting

transducers are placed in the space between gratings. This condition can be realized by using double electrode transducers or approximated by recessing aluminum electrodes in grooves etched into the quartz surface. The resonance condition is satisfied when the round trip phase shift is a multiple of 2π :

$$2\phi - 4\pi L_S / \lambda = 2n\pi \qquad (7)$$

Note that since ϕ equals π at the first zero in case d), any finite L_S results in satisfying the resonance condition in (7) at two values of λ removed from the center frequency with non-zero reflection coefficient. Thus, any simple resonator will exhibit at least three resonant modes, although the amplitudes of the "adjacent" modes at $n\pm1$ depend on R and on transducer placement.

At the grating resonant frequency, $\phi = 0$ and (7) reduces to

$$-4\pi L_S / p = 2m\pi \qquad (8)$$

where $m = n\pm1$. Combining (7) and (8) using (2) we obtain the resonance condition for the adjacent modes

$$DL_S = \phi(D) + \pi \qquad (9)$$

where

$$\phi\ (D) = \tan^{-1}(\ -\ D\ \tanh(GL_R)\ /\ G\ ) \qquad (10)$$

Simplification yields the resonance criterion

$$\tan(DL_S)\ /\ DL_R = -\ \tanh(GL_R)\ /\ GL_R \qquad (11)$$

Figure 2 shows the adjacent mode frequency in terms of D/K as a function of the normalized grating spacing KL_S for typical values of KL_R. Note that the y-intercept for each curve corresponds to the frequency of the first zero in R. The main result of the data in Fig. 2 is that an arbitrary grating spacing can be utilized with arbitrary suppression of the adjacent modes, at the cost of reducing K and increasing L_R. As noted by Stevens, et al. [2], the adjacent cavity modes have symmetry opposite the primary mode with respect to the center of the cavity. Thus, the first adjacent modes can be effectively suppressed for any cavity length by properly positioning the transducers within the cavity. Figure 3 shows one possible two port resonator topology requiring reflectionless transducers that effects this suppression. Although the interconnection of the split transducer is an annoyance, it is hardly prohibitive. As shown in Fig. 2, the second set of adjacent modes having the same symmetry as the primary mode are not troublesome for any reasonable cavity length.

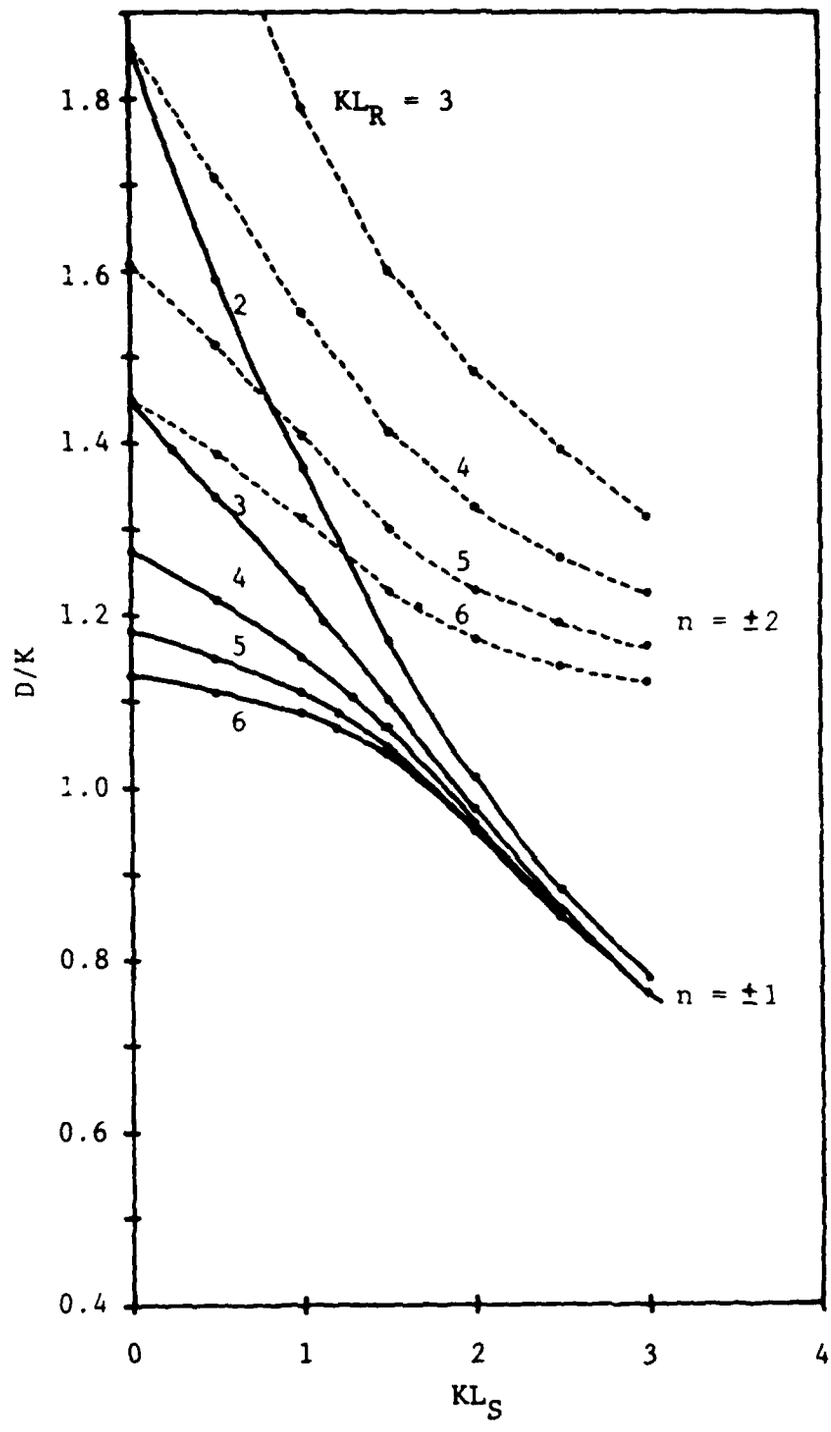

Figure 2. Adjacent mode frequency (D/K) as a function of KL_S for typical values of KL_R.

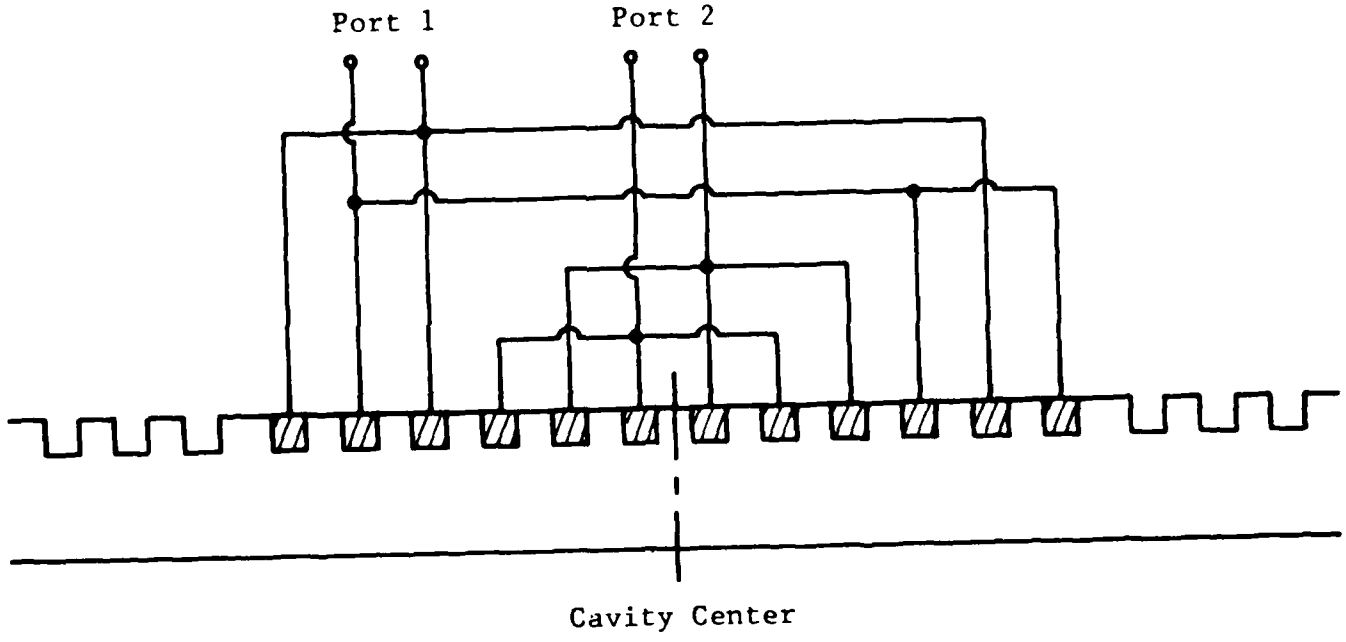

Figure 3. Resonator structure having symmetric placement of transducers to suppress adjacent cavity modes.

A more complicated situation exists in the case in which the transducers are reflecting. In this situation, the position of the transducers relative to the grating is fixed such that all reflections are in phase. With this constraint it is not possible to position the transducer electrodes at the peaks of the cavity standing wave. Thus coupling to the primary mode is reduced and coupling to adjacent modes is assured. However, the effective cavity spacing is small, reducing the excitation of these spuria to insignificant levels. The distortion of the transducer response due to internal reflections is of substantial importance.

The structure of interest is shown in Fig. 4a. The transducers are each of length L_T = Mp, and are synchronous with the gratings of length L_R. Again employing a coupling of modes analysis, the transfer coefficient from the electrical port to the forward acoustic port of a single grating and transducer is given by

$$A = jaVe^{-jDL_T}[(1-jR)(D-K)(\cosh(GL_T)-1)-jG(1+jR)\sinh(GL_T)] \quad (12)$$
$$G[G\cosh(GL_T) + j(D+jKR)\sinh(GL_T)]$$

where a is the electromechanical excitation constant, V is the terminal voltage, and R is the reflection coefficient of the grating given in (1). If the source and load are lightly coupled, then the reponse of a two port resonator can be evaluated using the diagram in Fig. 4b where the electrical

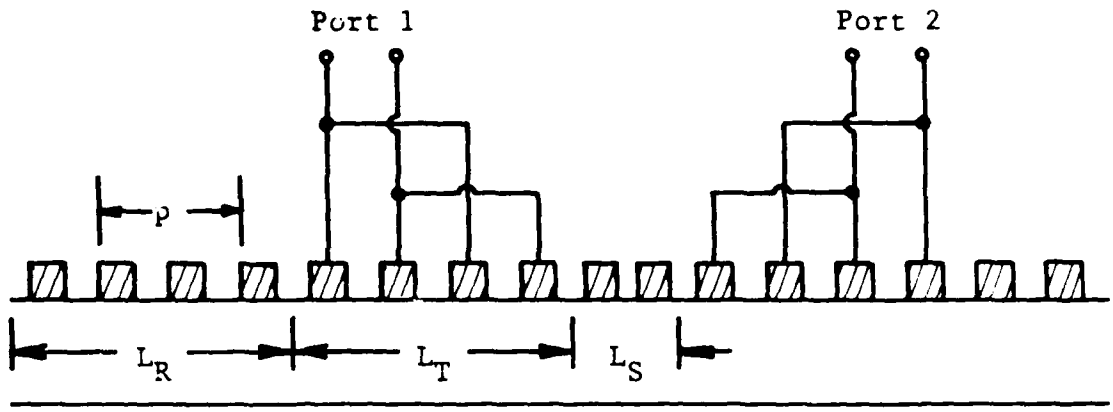

a.)

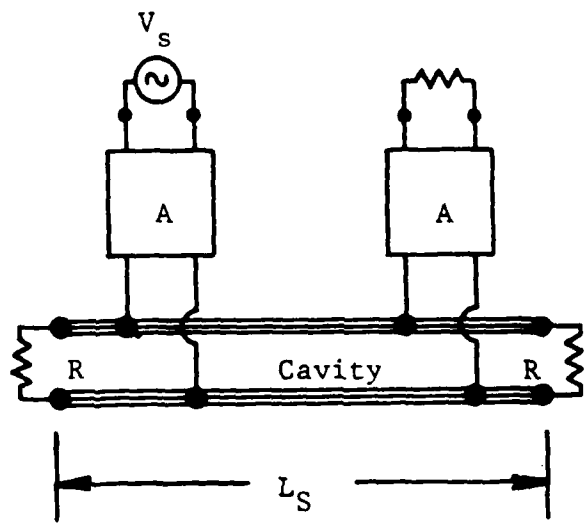

b.)

Figure 4. a.) Resonator structure having reflective transducers. b.) Equivalent transmission line network.

ports are coupled to the resonant cavity through the transfer coefficient in (12). Figure 5 shows the magnitude of (12) for various values of L_T, but keeping L_T+L_R constant. The stripe reflection constant, K, is taken to correspond to an aluminum film having a thickness of 2% of the acoustic wavelength on ST quartz, and the plots have been normalized to the value of the transfer coefficient for a reflectionless transducer of length L_T at its center frequency. Note that although the magnitude of the low frequency spurious is approximately constant, the value of the transfer coefficient at D=0 varies considerably.

The low frequency spurious occurs at a frequency for which jR is real, resulting in nearly complete reflection of the backward generated wave in synchronism with the forward wave. Thus the magnitude of the spurious is approximately 2, and it occurs at a value of D given approximately in (5). Since R is approximately unity at D=0, the peak magnitude at D=0 is $2^{1/2}$. However, in long transducers a portion of the energy is trapped within the transducer due to mechanical reflections, and the response at D=0 diminishes. Evaluation of (12) yields an expression for the ratio of the response at the low frequency spurious to the response at D=0

$$|B| = 2^{1/2} KL_T / (1 - \exp(-KL_T)) \qquad (13)$$

As in the case of longitudinal mode generation, it is

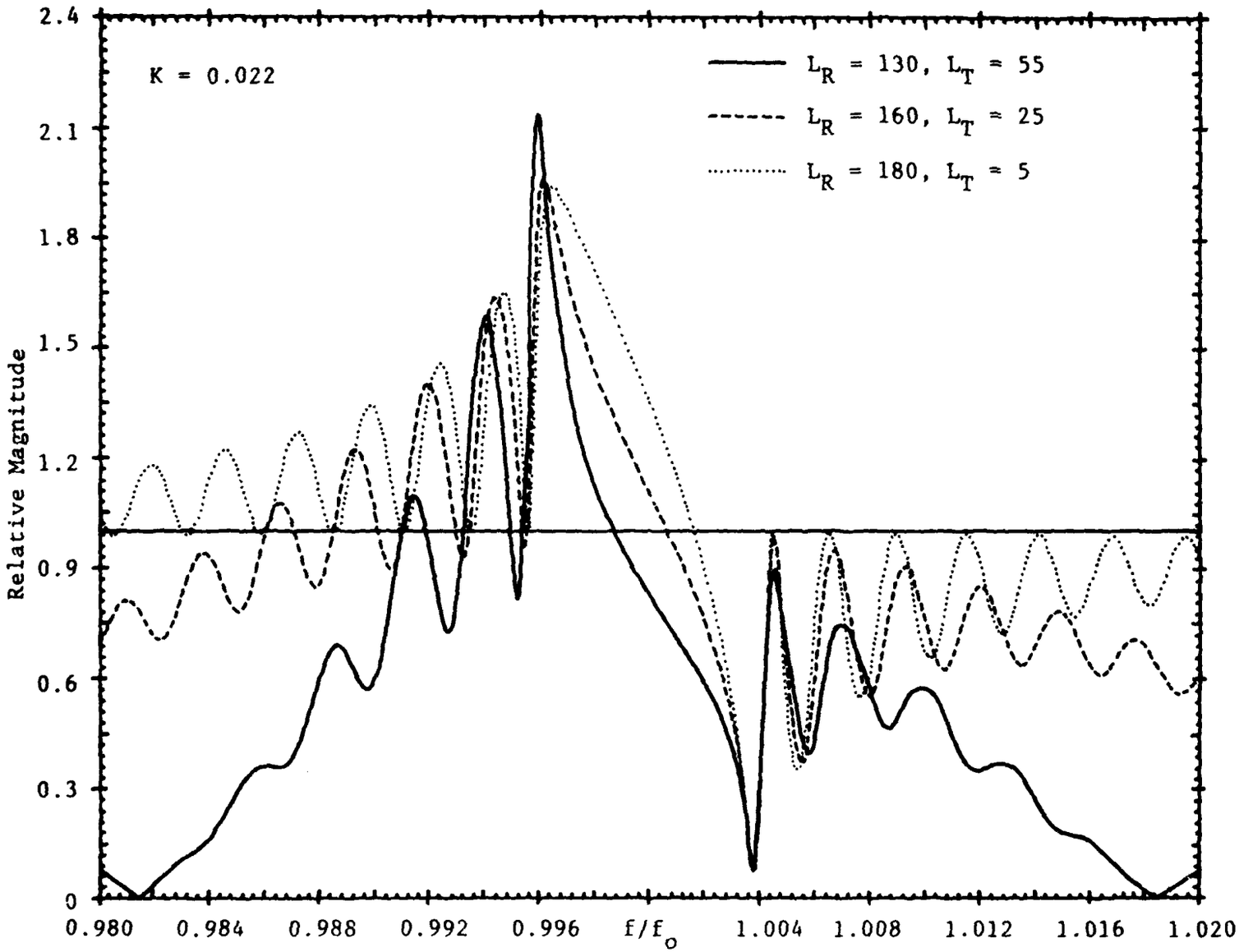

Figure 5. Magnitude of the forward transfer coefficient

possible to reduce the relative amplitude of the spurious response by reducing K, but at the expense of increasing L_R to maintain a given Q.

Examination of equations (1) and (12) shows that the frequency dependence of both can be expressed solely in terms of D/K. Thus, changing the sign of K results in reversing the frequency dependence about D=0. The acoustic impedance of gold is substantially higher than that of ST quartz, resulting in a K having opposite sign to that observed for aluminum. Based on the results above, it would be expected that resonators fabricated with gold and aluminum would have complementary frequency response functions apart from the primary resonance. Figure 6 compares the response of two 150MHz two port resonators having identical topologies (as in Fig. 4), but fabricated with aluminum and gold metallizations. The observed frequency response functions are in agreement with expectations. Note that a bimetal resonator structure could be constructed that would result in a symmetric response having low off resonance spuria. The challenge of adjusting metal thicknesses to precisely match SAW velocities in the two sections is considerable.

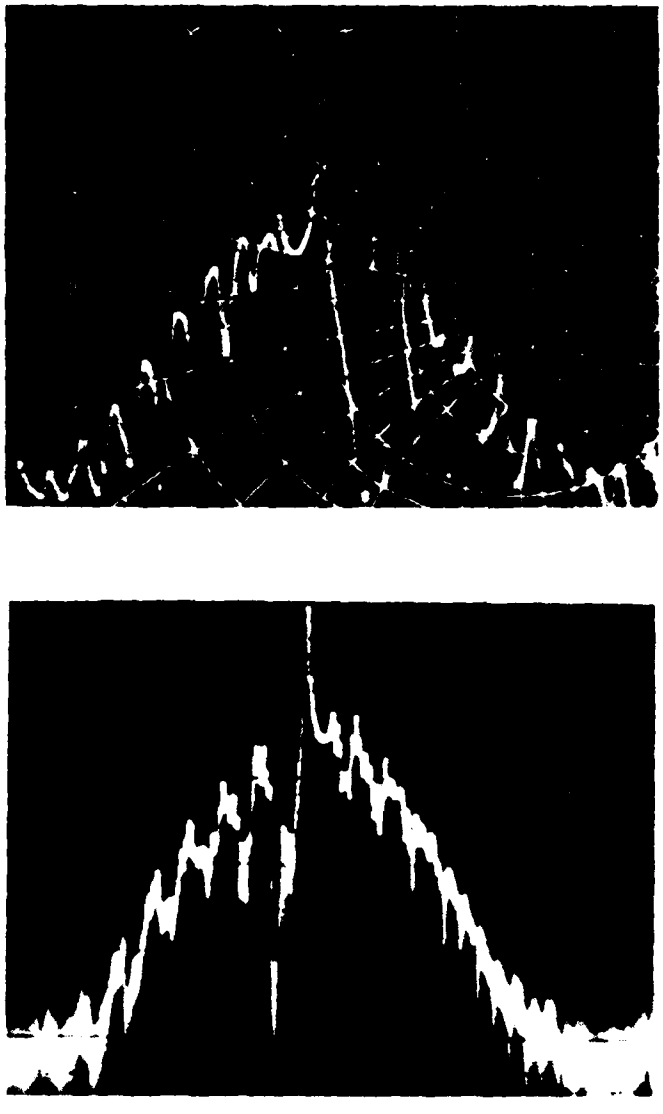

Figure 6. Top: aluminum metal cavity resonator response, vertical 10 dB/div, horizontal 1 MHz/div. Bottom: gold metal cavity resonator response, vertical 10 dB/div, horizontal 1.5 MHz/div.

References

[1] P. V. Wright and H. A. Haus, 'Theoretical Analysis of Second-Order Effects in Surface Wave Gratings, ' Proc. 34th Ann. Freq. Control Symposium, Ft. Monmouth N.J., pp. 262-268.

[2] R. Stevens, P. D. White, R. F. Mitchell, P. Moore and M. Redwood, 'Stopband Level of 2-port SAW Resonator Filters, ' Proc. 1977 Ultrasonics Symposium, IEEE Catalog No. 77CH1264-1SU, pp. 905-908.

APPENDIX II

An Analysis of SAW Interdigital Transducers With Internal Reflections and the Application to the Design of Single-Phase Unidirectional Transducers

AN ANALYSIS OF SAW INTERDIGITAL TRANSDUCERS WITH INTERNAL REFLECTIONS AND THE APPLICATION TO THE DESIGN OF SINGLE-PHASE UNIDIRECTIONAL TRANSDUCERS

C. S. Hartmann, P. V. Wright, R. J. Kansy, and E. M. Garber +
RF Monolithics, Inc.
Dallas, Texas

Abstract

A new coupling-of-modes (COM) analysis of SAW interdigital transducers (IDTs) is presented. The analysis includes the effects of multiple reflections within a transducer. The fundamental equations are derived and some simple closed-form results are given. In addition, some general properties having regard to the relative phase of transduction and reflection coefficients within a transducer are derived. A new class of unidirectional transducers is proposed which require only one matching network and do not have the crossovers required in current three-phase designs. These single-phase unidirectional transducers (SPUDTs) utilize internal reflections within the transducer to achieve unidirectional behavior. Practical SPUDT configurations are proposed and some experimental results presented. The application of the new COM analysis to synthesis is discussed.

Introduction

Lumped element models can be used to analyze SAW IDTs with the inclusion of internal reflections.[1] However, since such analyses are numerical in nature, they cannot be applied to the problems of synthesis. Current synthesis techniques for SAW transducers assume that internal reflections within a transducer are small enough to be neglected.[2] Internal transducer reflections are generally undesired and therefore split-finger or recessed electrode configurations are employed to eliminate them. However, requiring "a priori" that there be no internal reflections everywhere within a transducer removes an additional degree of freedom in the design. We seek to demonstrate in this paper that such reflections, if properly controlled, can be used to advantage. More specifically they may be used to achieve unidirectional behavior in a single-phase transducer.

The design of transducers with strong internal reflections requires a new analysis of SAW IDTs which gives closed-form solutions that can be inverted for synthesis. We believe that COM theory has the greatest potential for achieving this objective. COM theory has been extensively applied to the design of optical devices.[3,4] However, it has found only infrequent application in the field of SAW devices. Recently, however, the power of COM theory in analyzing SAW grating structures was demonstrated.[5,6] In this paper, that analysis is expanded upon to include transduction. The new theory can be used to obtain exact, or approximate closed-form solutions for the response of a transducer with strong internal reflections. The latter can then be used for synthesis.

This paper proposes for the first time a new class of transducers, namely single-phase unidirectional. By appropriately controlling the amplitude and phase of the reflection coefficient in a transducer unidirectional behavior can be realized. The new COM analysis can be used to understand and synthesize such a transducer. These transducers should find widespread application in low-loss filter applications.

Theory

Fundamental Equations

For generality, we shall consider a SAW transducer in which reflections are caused both by the electrode fingers and also by a reflective grating within the transducer [Fig.1b]. We shall assume that the nature of the reflective strips is such that they have no effect on transduction. In addition, we shall assume that the ratio of the local grating period to the local transducer period is a constant. By displacing the reflective grating with respect to the transducer electrodes the phase of the local reflection coefficient in the transducer may be varied relative to the transduction coefficient. Later in the paper, we shall propose some practical configurations for achieving the desired phase shift.

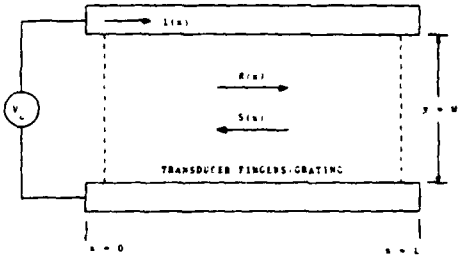

FIG. 1a Transducer Configuration for the COM Analysis

For simplicity we shall assume that the transducer is uniform in the transverse (y) direction, i.e. no overlap weighting. We shall also assume that the transducer is sufficiently wide that diffraction effects can be ignored. With these assumptions, the analysis problem becomes one dimensional with a dependence on x alone. A set of partial differential COM equations can be written to describe the full two dimensional problem. However, the equations are necessarily more complex and will not be considered in this paper.

+ Present Address: MIT, Cambridge, MA 02139

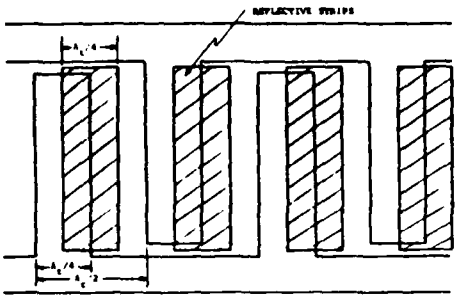

FIG. 1b SAW Transducer with an Internal Reflective Grating

Likewise, both propagation loss and finger loss will be ignored.

The COM equations for a transducer are best introduced by first considering the case in which the transducer [Fig.1a] is short circuited. The equations for the forward and reverse propagating wave amplitudes R(x) and S(x) respectively are

$$\frac{d}{dx}\tilde{R}(x) = -j\left[K(x)e^{2j\phi_k}\right]e^{2j\phi(x)}\tilde{S}(x) \quad (1)$$

$$\frac{d}{dx}\tilde{S}(x) = j\left[K(x)e^{-2j\phi_k}\right]e^{-2j\phi(x)}\tilde{R}(x) \quad (2)$$

if R(x) and S(x) are symmetric variables. Here $\tilde{R}(x)$ and $\tilde{S}(x)$ are slowly varying wave amplitudes defined by

$$R(x) = \tilde{R}(x)\, e^{j(\omega t - k_t x)}$$

$$S(x) = \tilde{S}(x)\, e^{j(\omega t + k_t x)}$$

where ω is the angular frequency and k_t is the mean propagation constant under the transducer. The phase detuning is

$$2\phi(x) = 2\left[k_t x - \int_o^x dx'(2\pi/\Lambda_t(x))\right] \quad (3)$$

where $\Lambda_t(x)$ is the period of the transducer. K(x) is the coupling coefficient/unit length between the two counterpropagating waves [not to be confused with the electromechanical coupling coefficient (k^2) which is absorbed in the transduction function α described later]. In general it is a result of both the reflective grating and the transducer electrodes. In a lossless transducer K(x) is the magnitude of the coupling coefficient/unit length with the phase angle given by

$$2\phi_k = 2\,(2\pi/\Lambda_t(0))X \quad (4)$$

where X is the displacement, in the +x direction, of the first effective center of reflection from the origin (x=0).

The full COM equations for a transducer grating configuration such as that shown in Fig. 1 are now obtained by adding transduction terms to the shorted grating equations ((1) and (2)). In addition, a third equation is required for the current along the transducer I(x). The origin will be taken at the center of the first electrode finger, or group of split-fingers. If the voltage across the transducer is V_o the transducer equations have the general form

$$\frac{d}{dx}\tilde{R}(x) = -j\left[K(x)\,e^{2j\phi_k}\right]e^{2j\phi(x)}\tilde{S}(x) - j\alpha(x)e^{j\phi(x)}V_o$$

$$\frac{d}{dx}\tilde{S}(x) = j\left[K(x)e^{-2j\phi_k}\right]e^{-2j\phi(x)}\tilde{R}(x) + j\alpha(x)e^{-j\phi(x)}V_o$$

$$\frac{d}{dx}I(x) = -j\omega C(x)V_o + \beta_1(x)\,\tilde{R}(x) + \beta_2(x)\,\tilde{S}(x)$$

where C(x) is the capacitance/unit length of the transducer. The term $\alpha(x)$ is the transduction coefficient/unit length in the transducer. Reciprocity and power conservation can be used to relate the coefficients $\alpha(x)$, $\beta_1(x)$ and $\beta_2(x)$. Reciprocity requires that the scattering matrix of the equivalent three-port network for an incremental section of the transducer is symmetrical. This requirement leads to

$$\beta_1(x) = -2j\alpha(x)e^{-j\phi(x)}$$

$$\beta_2(x) = -2j\alpha(x)e^{j\phi(x)}$$

Power conservation then implies

$$\alpha^*(x) = \alpha(x)$$

Thus $\alpha(x)$ must be pure real. The COM equations for a lossless transducer with internal reflections are therefore

$$\frac{d}{dx}\tilde{R}(x) = -j\left[K(x)e^{2j\phi_k}\right]e^{2j\phi(x)}\tilde{S}(x) - j\alpha(x)e^{j\phi(x)}V_o \quad (5)$$

$$\frac{d}{dx}\tilde{S}(x) = j\left[K(x)e^{-2j\phi_k}\right]e^{-2j\phi(x)}\tilde{R}(x) + j\alpha(x)e^{-j\phi(x)}V_o \quad (6)$$

$$\frac{d}{dx}I(x) = -j\omega C(x)\,V_o - 2j\alpha(x)\,e^{-j\phi(x)}\,\tilde{R}(x) - 2j\alpha(x)\,e^{j\phi(x)}\tilde{S}(x) \quad (7)$$

where K(x) and $\alpha(x)$ are pure real. Uncoupling $\tilde{R}(x)$ and $\tilde{S}(x)$ from (5) and (6) gives the following equations for the counterpropagating waves in the transducer

$$\tilde{R}''(x) - \left[\frac{K'(x)}{K(x)} + 2j\phi'(x)\right]\tilde{R}'(x) - K^2(x)\,\tilde{R}(x) = V_o e^{j\phi(x)}\left[\alpha(x)K(x)e^{2j\phi_k} - j\,\alpha'(x) - j\alpha(x)\left(\frac{K'(x)}{K(x)} + j\phi'(x)\right)\right] \quad (8)$$

$$\tilde{S}''(x) - \left[\frac{K'(x)}{K(x)} - 2j\phi'(x)\right]\tilde{S}'(x) - K^2(x)\tilde{S}(x) = V_o e^{-j\phi(x)}\left[\alpha(x)K(x)e^{-2j\phi_k} + j\,\alpha'(x) - j\alpha(x)\left(\frac{K'(x)}{K(x)} - j\phi'(x)\right)\right] \quad (9)$$

where the prime denotes differentiation with respect to x. The boundary conditions for the

waves are

$$\tilde{R}(o) = 0 \qquad \tilde{S}(L) = 0$$

$$\tilde{R}'(L) = -j\alpha(L)\, e^{j\phi(L)}\, V_o \qquad \tilde{S}'(o) = j\alpha(o)\, V_o \qquad (10)$$

where the transducer occupies the region $0 \leq x \leq L$.

Application

If the coupling coefficient $K(x)$ in a transducer is a constant, i.e. K_o, and the transducer period is constant, equations (8) and (9) for the counterpropagating waves can be solved exactly. This holds for any arbitrary transduction function $\alpha(x)$. Expressions for the outgoing waves $R(L)$ and $S(0)$, for this case, can be obtained in closed form. In addition, the transducer input admittance $Y = I(0)/V_o$ can also be obtained from equation (7). These solutions would apply to a withdrawal-weighted transducer with dummy fingers. As verification of our theory, we present here the closed form expression obtained for the input conductance of an unweighted constant-period transducer with 2 fingers/wavelength.

For the general case in which reflections are caused both by the transducer electrodes and by an internal grating, [Fig.1b] the conductance is

$$G = \frac{8\alpha_o^2 \sinh^2(\beta L/2)\left[K_o(K_o - \Delta\cos 2\phi_k)\cosh\beta L + \Delta(K_o\cos 2\phi_k - \Delta)\right]}{(K_o^2 - \Delta^2)\,(K_o^2\cosh^2\beta L - \Delta^2)} \qquad (11)$$

where α_o is the transduction coefficient and Δ represents the detuning from synchronism. We have $\beta(x) = \beta x$, thus from (3)

$$\Delta = k_t - 2\pi/\Lambda_t$$

also

$$\beta = (K_o^2 - \Delta^2)^{1/2}$$

Note that the input conductance at synchronism ($\Delta = 0$) is *independent of* the phase shift ϕ_k between the transduction and reflection coefficients. For the simple case of a transducer with no internal grating, reflections are due only to the electrode fingers, thus $\phi_k = 0$. The input conductance is then

$$G = \frac{8\alpha_o^2 \sinh^2(\beta L/2)(K_o\cosh\beta L + \Delta)}{(K_o + \Delta)(K_o^2\cosh^2\beta L - \Delta^2)} \qquad (12)$$

This expression, normalized to the idealized conductance in the absence of reflections, is plotted in Fig. 2a for the *same* transducer parameters that were analyzed using an equivalent circuit model in ref. 1. For comparison the theoretical and experimental results from ref. 1 are shown in Fig. 2b. Agreement with the lumped element analysis and experiment is seen to be very good, except for the shift in center frequency due to mass-loading and stored-energy effects which have been ignored here for simplicity.

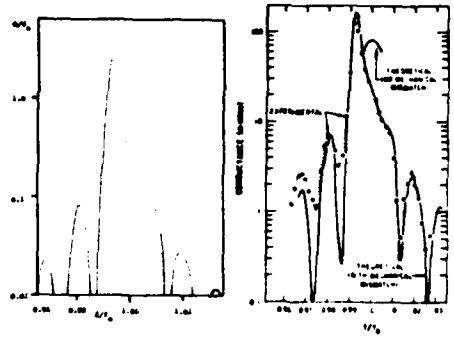

FIG. 2a Conductance of a 78-Finger Pair Transducer
2b Results from Reference 1

Equations (8) and (9) can also be used to determine the effect of varying the phase angle ϕ_k between the centers of reflection and transduction within a transducer. In a transducer with a symmetric transduction function $\alpha(x) = \alpha(L-x)$ and a symmetric reflection coefficient $K(x) = K(L-x)$ it can be shown that for a symmetric response, i.e. $R(L-x) = S(x)$, we require $\phi_k = 0$. This is the case in a conventional transducer with no internal reflective grating. If $\phi_k \neq 0$, however, even in a transducer which is otherwise totally symmetric the forward and reverse propagating waves are in general not of the same magnitude. This result suggests the exciting possibility of using internal reflections within a transducer to enhance the wave transduced in one direction at the expense of the wave transduced in the reverse direction. The best choice of ϕ_k for achieving such unidirectional behavior is relatively straightforward.

Consider a transducer with a uniform transduction coefficient $\alpha(x) = \alpha_o$ and a uniform coupling coefficient $K(x) = K_o$. The solutions for the outgoing waves, from (8), (9) and (10) are

$$\tilde{R}(L) = \frac{\alpha_o V_o e^{j\Delta L}\left[(\Delta - K_o e^{2j\phi_k})(\cosh\beta L - 1) - j\beta\sinh\beta L\right]}{\beta\,(\beta\cosh\beta L + j\Delta\sinh\beta L)}$$

$$\tilde{S}(o) = \frac{\alpha_o V_o\left[(\Delta - K_o e^{-2j\phi_k})(\cosh\beta L - 1) - j\beta\sinh\beta L\right]}{\beta\,(\beta\cosh\beta L + j\Delta\sinh\beta L)}$$

At center frequency ($\Delta = 0$) the directivity of the transducer is thus

$$\left[\frac{\tilde{R}(L)}{\tilde{S}(o)}\right]^2 = \left[\frac{e^{2j\phi_k} + j\coth(K_o L/2)}{e^{-2j\phi_k} + j\coth(K_o L/2)}\right]^2 \qquad (13)$$

This expression is clearly a maximum when $\phi_k = \pi/4$ (assuming $K_o > 0$). From (4) to achieve maximum unidirectionality the centers of reflection

in the transducer must therefore be displaced a distance $X = \Lambda_t/8$ from the centers of reflection. This result is also intuitively obvious. Consider a transducer with split-finger electrodes and an internal grating displaced $\Lambda_t/8$ in the $+x$ direction from the centers of each finger pair [Fig. 3]. If, as in the configuration of Fig. 1, the reflecting strips do not interfere with transduction, the centers of transduction correspond to the centers of the split fingers. In the transducer, the centers of reflection coincide with the centers of the reflecting strips, since the split-finger electrodes do not contribute to the reflection coefficient. From the COM equations (1) and (2) in the case of no loss, the acoustic reflection coefficient at the center of each reflecting strip is $-jK_o$ at synchronism. For simplicity we now consider the acoustic waves generated by a single split-finger pair in the transducer. If the reflective strips are all displaced a distance $x = \Lambda_t/8$ from the centers of the split fingers, the reflections of the forward acoustic wave, in the reverse direction are all out of phase with the direct wave transduced in the reverse direction [Fig. 3]. In contrast, the reflections of the reverse propagating wave in the forward direction, are all in phase with the direct wave transduced in the forward direction. Thus, the wave transduced in the reverse direction is attenuated as a result of destructive interference whereas that in the forward direction is enhanced as a result of constructive interference. If $K_o < 0$, the direction of unidirectionality is reversed.

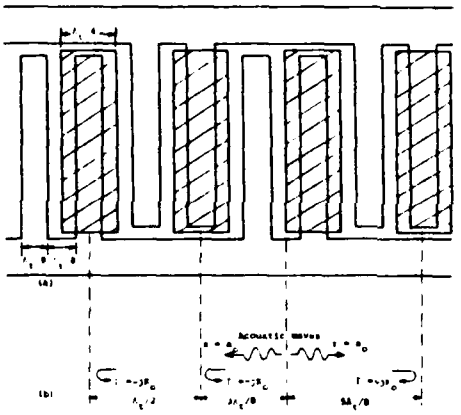

FIG. 3a Split-Finger Transducer with Internal Grating Shifted by $\Lambda_t/8$.
3b Acoustic Reflections in Transducer

We may obtain an estimate of the magnitude of the coupling coefficient from (13). With $\phi_o = \pi/4$ the directivity of a simple SPUDT at center frequency, with constant α_o and K_o is

$$\left[\frac{\cosh(K_oL/2) + \sinh(K_oL/2)}{\cosh(K_oL/2) - \sinh(K_oL/2)}\right]^2$$

$$= e^{2K_oL} = 8.69\,K_oL \text{ dB}$$

Thus, for example, with $K_oL = 1$ we may achieve a peak directivity at center frequency from such a transducer of 8.69 dB. A filter comprised of two such transducers, under matched conditions, would have a minimum insertion loss of only 1.1 dB with a triple transit suppression level of -37 dB.

From (11) we may determine the input conductance of a simple SPUDT (i.e. constant period, α_o, K_o). The input conductance is

$$G = \frac{8\alpha_o^2 \sinh^2(BL/2)(K_o^2\cosh BL - \Delta^2)}{(K_o^2 - \Delta^2)(K_o^2\cosh^2 BL - \Delta^2)}$$

At center frequency the conductance is unchanged from the bidirectional case (eq. (12)). However, the conductance of the SPUDT is totally symmetric about the center frequency f_o. In Fig. 4, the conductance is plotted of a SPUDT, with the same parameters as the bidirectional transducer of Fig. 2.

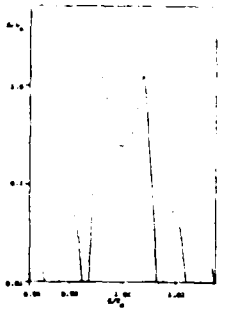

FIG. 4 Conductance of Constant-Period Unweighted SPUDT.

To achieve desired passband and side-lobe characteristics with a SPUDT, in general, requires the synthesis of a spatially dependent coupling coefficient K(x). Later we shall discuss how the COM analysis, presented here, may be applied to such a synthesis. However, first we propose a practical configuration for a SPUDT and present some experimental results.

A Practical SPUDT

The drawback to the SPUDT structures shown in Fig. 1 and Fig. 3, is that the reflective strips must be either an insulating overlay, or indiffused or ion implanted region so as not to shift the centers of transduction. In addition, with two fingers/wavelength as in Fig. 1 if the electrode fingers are not recessed reflections from the fingers will cause a shift at the centers of

reflection away from the centers of the reflective strips. The centers of reflection and transduction must be accurately known so that the desired phase shift $\phi_k = \pi/4$ can be maintained throughout the SPUDT.

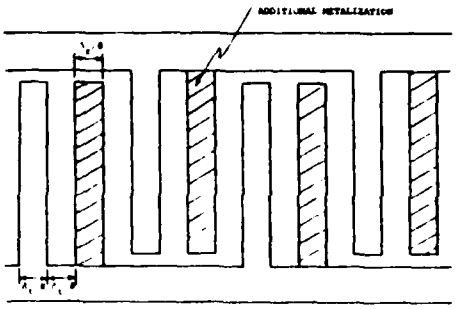

FIG. 5 Practical Configuration for a SPUDT.

A practical configuration for a SPUDT is shown in Fig. 5. Split-finger electrodes are utilized and the internal reflections are achieved by additional mass loading of alternate fingers. The mass loading simply requires an additional metallization step. In such a structure, *transduction and reflection are totally separate* and controllable functions. The split-finger electrodes cause no reflections and the mass loading does not affect transduction. The displacement in this structure between the centers of reflection and transduction is thus exactly $\lambda_t/8$ as desired everywhere in the transducer, regardless of $K(x)$.

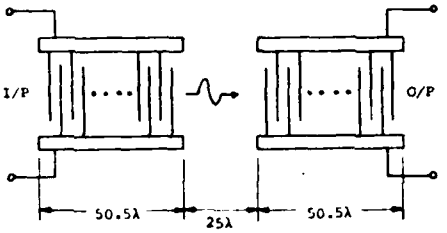

FIG. 6 Filter Configuration.

To verify the concept and analysis of a *SPUDT*, a simple prototype filter was fabricated on *ST-quartz*. The filter comprised two identical SPUDTs with constant period, α_p and K_p, in the configuration shown in Fig. 6. The two SPUDTs were fabricated as proposed in Fig. 5, with gold being used for the second level of metalization. For *comparison*, an identical structure was also fabricated without the second level metalization. In the latter device, the two transducers were therefore bidirectional. Experimental measurements of the performance of the filter with the two SPUDTs are presented in Fig. 7. The filter was tuned for minimum insertion loss at center frequency. As the matched condition was approached the level of triple transit suppression in the *filter increased*. In contrast, the triple transit suppression degraded, as expected, in the filter employing the bidirectional transducers as it was tuned to a matched condition. The triple transit level in the SPUDT filter was -25 dB compared with only -20 dB in the filter with bidirectional transducers. At the same time, the minimum insertion loss was approximately 6 dB lower. The SPUDT filter had a minimum insertion loss of approximately 6.5 dB whereas the filter with bidirectional transducers had a minimum insertion loss of approximately 12.6 dB. Both insertion losses are higher than was expected as a result of a problem with surface contamination. However, the experimental results clearly demonstrate the *superior performance characteristics* and practical realizability of a SPUDT.

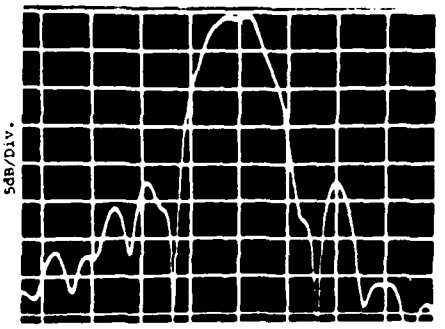

FIG. 7a SPUDT Filter Insertion Loss.

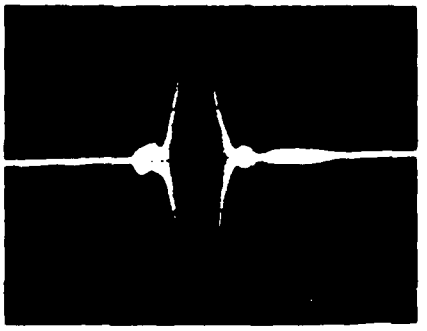

FIG. 7b Triple-Transit Response.

SPUDT Synthesis

The synthesis of a SPUDT with desired performance characteristics is a more complex procedure than that required for conventional transducers. In conventional bidirectional or three-phase unidirectional transducers, the only design variable is the transduction function $\alpha(x)$.

This implies that only one scattering parameter for the transducer can be specified. Usually the transfer function between the electrical and forward acoustic port is specified which results in a unique $\alpha(x)$. The reflection coefficient on the forward acoustic port, required to achieve a given level of triple-transit suppression, cannot be specified in addition. In a SPUDT, however, both $\alpha(x)$ and $K(x)$ are variables. Therefore, both a desired electro-acoustic transfer function and a desired acoustic reflection coefficient can be independently specified.

An approximate synthesis procedure has been developed for the design of transducers having 2 dB or more insertion loss. With this level of insertion loss the magnitude of the coupling coefficient required in the transducer remains relatively small. Approximate closed-form solutions which can be easily inverted can then be obtained from the COM equations. The synthesis of $K(x)$ is performed independently from $\alpha(x)$. From the specifications of a desired electro-acoustic transfer function and a desired reflection coefficient on the forward acoustic port the reflection coefficient on the forward acoustic port under short circuit conditions ($V_o = 0$) is determined. The required form of $K(x)$ is then determined from the COM equations (5) and (6) independently of $\alpha(x)$. Once the coupling coefficient has been determined the transduction function required to achieve the desired electro-acoustic transfer function can be obtained. Again approximate solutions to the COM equations are currently used. Work is presently continuing to develop a synthesis procedure for lower loss devices.

Summary

(1) We have developed a new COM analysis of SAW IDTs that includes the effects of internal reflections.

(2) Closed-form solutions to the COM equations can be obtained for simple transducers, approximate solutions for more complex structures.

(3) The closed-form expression obtained for the conductance of a constant-period unweighted transducer is in good agreement with experimental results.

(4) The COM analysis reveals that if the internal reflection centers are displaced by $\lambda_t/8$ from centers of transduction unidirectional behavior can be obtained from a single-phase transducer.

(5) A practical configuration for a SPUDT has been proposed and demonstrated.

(6) An approximate synthesis procedure for a SPUDT based on the COM analysis has been developed.

We believe that SPUDTs will find numerous applications in low-loss filters and other applications in the near future.

Acknowledgements

The authors gratefully acknowledge the assistance of H. A. Haus and the support of the National Science Foundation Grant No. ECS-8116654.

References

1. W. S. Jones, C. S. Hartmann, and T. D. Sturdivant, "Second Order Effects in Surface Wave Devices", IEEE Trans. Sonics and Ultrasonics, Vol. SU. 19, No. 3, 1972, 368 - 377.

2. C. S. Hartmann, D. T. Bell, Jr. and R. C. Rosenfeld, "Impulse Model Design of Acoustic Surface-Wave Filters", IEEE Trans. MTT, Vol. 21, No. 4, 1973, 162 - 175.

3. M. Masanori, K. O. Hill, and A. Watanabe, "Optical-Waveguide Filters: Synthesis", J. Opt. Soc. of Amer.), Vol. 65, No. 7, 1975, 804 - 809.

4. R. C. Alferness and P. S. Cross, "Filter Characteristics of Codirectionally Coupled Waveguides with Weighted Coupling", IEEE J. Quant. Elec., Vol. QE-14, No. 11, 1978, 843 - 847.

5. P. V. Wright and H. A. Haus, "Theoretical Analysis of Second-Order Effects in Surface-Wave Gratings", Proc. 34th Ann. Freq. Control Symp., 1980.

6. P. V. Wright and H. A. Haus, "A Closed-Form Analysis of Reflective-Array Gratings", Ultrason. Symp. Proc., 1980, 282 - 287.

DISTRIBUTION LIST

Advisory Group on Electron Devices
201 Varick Street
New York, NY 10014 (1)

RADC (EEA)
L.G. Hanscom Field
Bedford, MA 01731
Attn: Dr. P. Carr (1)

Commander
Naval Electronic Systems Command
Washington, D.C. 20360
Attn: Code 614 (J.A. Cauffman) (1)
Code 614 (J.P. Letellier) (1)

Commander
Naval Air Systems Command
Washington, D.C. 20360
Attn: AIR 33 (C. Caposell) (1)

Defense Technical Information Center
Building 5, Cameron Station
Alexandria, VA 22314 (12)

U.S. Army Electronics Technology Devices Laboratory
(ERADCOM)
Delet-MA-M
Fort Monmouth, N.J. 07703
Attn: T. Lukasek (1)

Commanding Officer
Naval Research Laboratory
Washington, D.C. 20375
Attn: Code 6853 (D.C. Webb) (15)

SAWTEK, Inc.
P.O. Box 7756
2451 Shader Road
Orlando, Florida 32854
Attn: Mr. S. Miller (1)

Raytheon Company
Research Division
28 Seyon Street
Waltham, Massachusetts 02154
Attn: Dr. M.B. Schulz (1)

Sperry Rand Research Center
100 North Road
Sudbury, Massachusetts 01776
Attn: Dr. H. Van De Vaart (1)
Mr. P.C. Meyer (1)


DA
FIL